

Simulating rough surfaces by periodic and biperiodic gratings

Andreas Rathsfeld

submitted: December 23, 2022

Weierstrass Institute
Mohrenstr. 39
10117 Berlin
Germany
E-Mail: andreas.rathsfeld@wias-berlin.de

No. 2989
Berlin 2022



2020 *Mathematics Subject Classification.* 35P25, 74J20, 76B15, 78A45, 78A46.

Key words and phrases. Scattering problem, Dirichlet problem, Helmholtz equation, radiation condition, stochastic rough surface, Bayesian inversion, surrogate model.

Edited by
Weierstraß-Institut für Angewandte Analysis und Stochastik (WIAS)
Leibniz-Institut im Forschungsverbund Berlin e. V.
Mohrenstraße 39
10117 Berlin
Germany

Fax: +49 30 20372-303
E-Mail: preprint@wias-berlin.de
World Wide Web: <http://www.wias-berlin.de/>

Simulating rough surfaces by periodic and biperiodic gratings

Andreas Rathsfeld

Abstract

The scattering of acoustic and electro-magnetic plane waves by rough surfaces is the subject of many books and papers. For simplicity, we consider the special case, described by a Dirichlet boundary value problem of the Helmholtz equation in the half space above the surface. We recall the formulae of the far-field pattern and the far-field intensity. The far-field can be defined formally for general rough surfaces. However, the derivation as asymptotic limits works only for waves, which decay for surface points tending to infinity. Comparing with the case of periodic surface structures, it is clear that the rigorous model of plane-wave scattering is accurate for the near field close to the surface. For the far field, however, the finite extent of the beams in the planes orthogonal to the propagation direction is to be taken into account. Doing this rigorously, leads to extremely expensive computations or is simply impossible. Therefore and to enable the approximation of waves above the rough surface by waves above periodic and biperiodic rough structures, we consider a simplified model of beams. The beam is restricted to a cylindrical domain around a ray in propagation direction, and the wave is equal to a plane wave inside of this domain and to zero outside. Based on this beam model, we derive the corresponding asymptotic formulae for the wave and its intensity. The intensity is equal to the formally defined far-field intensity multiplied by a simple cosine factor. Under special assumptions, the intensity for the rough surface can be approximated by that for rough periodic and biperiodic surface structures. In particular, we can cope with the case of shallow roughness, where the reflected intensity includes, besides the smooth density function w.r.t. the angular direction, a plane-wave beam propagating into the reflection direction of the planar mirror.

Altogether, the main point of the paper is to fix the technical assumptions needed for the far-field formula of a simple beam model and for the approximation by the far fields of periodized rough surfaces. Furthermore, using the beam model, we discuss numerical experiments for rough surfaces defined as realizations of a random field and, to get a more practical case, the Dirichlet condition is replaced by a transmission condition. The far-field intensity function for a rough surface is the limit of intensity functions for periodized rough surfaces if the period tends to infinity. However, almost the same intensity function can be obtained with a fixed period by computing the average over many different realizations of the random field. Finally, we present numerical results for an inverse problem, where the parameters of the random field are sought from measured mean values of the intensities.

1 Introduction

Rough surfaces appear in many applications. We consider surfaces defined as the graph of continuous functions, which might be even smooth. By roughness we only indicate that the planar surface is perturbed by corrugations in a non-systematic way. These rough surfaces could be e.g. the water surface of the ocean or the surface of a workpiece, which ideally should be planar but has corrugations due to imperfections in the manufacturing process. Especially, in technical applications based on electro-magnetic waves of smaller and smaller wavelengths, small corrugations become more and more “visible” by the waves and have an important impact on the functional behaviour of the devices.

The theory of scattering by rough surfaces has been analyzed by many authors. We mention here e.g. the books [3, 27, 37], [34], [26, Chapt. 7], the articles [29, 36], and the overview paper [13]. There exist papers on numerical methods based on “rule of thumbs”, methods under simplifying assumptions, and algorithms of rigorous Helmholtz and Maxwell solvers based e.g. on finite-element (FEM), boundary-integral (BEM), and finite-difference-time-domain (FDTD) methods combined also with stochastic models of the surface (cf. e.g. [32, 39], [2], the books mentioned above, [35], the topical review [38], and the similar case of bounded domains treated in [17–19]).

For simplicity, in this paper we consider the scattered field as the solution of the Helmholtz equation in the domain above the surface together with a Dirichlet boundary condition at the rough surface. The Dirichlet boundary data is the restriction of an incident plane-wave. Clearly, this is the accepted model for acoustic waves with sound-hard boundary conditions and, in the two-dimensional case, also for TE-polarized electro-magnetic waves. Existence and uniqueness of the reflected wave solution have been proved in two dimensions. We guess that the case of three-dimensional Maxwell equations is quite similar. For this and for the three-dimensional Helmholtz equation (i.e., for acoustic waves), we assume there are classes of functions such that, for any rough surface represented as the graph of a function in the class and for any plane wave incidence, the corresponding Dirichlet problem has a unique wave solution.

In general, the Dirichlet problem for the Helmholtz equation is an accurate model for the scattering of the plane wave by the rough surface. This is true, though, instead of a complete plane-wave, a realistic incoming wave is a beam with a cross section of finite extent. If the finite diameter of the cross section is much bigger than the wavelength, then the near field, where the beam meets the rough surface, is accurately described by the Dirichlet solution. The far-field picture, however, is different. Only for waves, decaying over the rough surface at infinity, an asymptotic formula for the far-field of the solution is well known, and, using this, an asymptotic formula for the intensity (flux of energy) of the wave field can be derived. These well-known formulae of the far-field can formally be generalized to the plane-wave case, for which there is no decay. Unfortunately, the meaning as a term in the asymptotics is lost.

Therefore, for an asymptotic analysis of the scattering by rough surfaces, we have to take into account that any realistic wave beam has a cross section of finite extent. For example, looking at the optical experiments of reflection by periodic grating structures with wavelength in the range of visible light, we see a light-beam of a diameter in the range of a millimeter arriving onto the grating structure, and a finite number of similar light-beams appear as reflection. No scattering into other angular direction can be seen. Since a rigorous determination of the beam waves requires huge domains of computation, we have to simplify the model. In this sense, our plane-wave scattering model is based on beams of cylindrical structure (cf. the comments on tapered incident fields in [38, Sect. 2.4] or think of a simplified long Gaussian beam, cf. [25]). The diameter of the cross section should be huge in comparison to the wavelength, but the beam model is considered in the far field at a distance to the reflecting surface, which is huge in comparison to the diameter. By the assumption of our simple model, the wave is equal to the plane wave inside the beam, equal to zero outside the beam, and the more difficult exact behaviour close to the beam boundary is neglected. The shape of the cross section is of no importance, and the size of the cross section can only effect some nonessential constants in the formulae. Using this model for periodic and biperiodic surface structures, i.e. for gratings, we get an asymptotic behaviour as seen in the experiments. The far-field intensity is the weighted sum of the Dirac delta functions at the directions of the propagating reflected plane-wave modes, and the weights are exactly the well-known efficiencies of these wave modes. Applying the same model to rough surfaces, the asymptotic intensity function (density w.r.t. direction) is like the intensity function, formally derived for plane waves of infinite extent, except for some multiplicative factor equal to constant times cosine of the inclination angle of the direction. The additional cosine is due to the fact that the cross section of

the beam in a fixed direction is cosine times the size of the highlighted area at the rough surface, from where the beam in the fixed direction originates.

As a consequence of the simplified model, if the rough surface is approximated by periodic or biperiodic rough grating surfaces, then smoothed asymptotic intensities of the gratings tend to the smoothed asymptotic intensity of the rough surface. If the asymptotic intensity is smooth, then the smoothed asymptotic intensities of the gratings approximate the asymptotic intensity of the rough surface. Although the nature of the reflected fields is different for rough surfaces (diffuse irradiation into all directions) and for periodic or biperiodic structures (finite number of plane-waves), we end up with a good approximation. Consequently, well-developed grating solvers can be used for roughness as well. In fact, for approximations, the periodic extension of a finite section of a rough surface (cf. e.g. [35] and [22] for a comparison with tapered waves) is more natural than the simple truncation (cf. e.g. [7,8]). There is no reason to believe that the convergence (local or in weighted Lebesgue spaces) of periodic and biperiodic solutions to the rough-surface solution should be worse than that in the case of approximation by finite sections. Furthermore, in the case of rough surfaces close to an ideal planar surface (corrugations of small height), there should be a plane-wave beam in the reflected wave propagating into the reflection direction of a planar mirror (cf. e.g. [32]). This beam can be incorporated into the model with beams of finite extent. By simulations based on a FEM for two-dimensional gratings, we demonstrate that such beams really appear besides the smooth density function of intensity. Note however, to get a more practical case, the Dirichlet boundary condition is replaced by a transmission condition in all our numerical examples.

Altogether, we employ a unified and simplified model for reflection by rough surfaces and by periodic surface structures, which is based on the exact near-field model close to the rough surface and on simple beam propagation up to the far field. This leads to the classical far-field picture for periodic and biperiodic surface structures. Approximating the rough surface by such gratings, we get the far-field intensity function of the waves reflected by rough surfaces. The two main objectives of the current paper are, on the one hand, to highlight the technical assumptions for the intensity formulae and for the approximation by periodized rough surfaces and, on the other hand, to demonstrate the convergence in numerical experiments. Note that the assumptions concern the unique solvability of the boundary value problem (cf. Asms. 2.1 and 3.1), the local convergence of the corresponding finite-section method (cf. Asm. 3.4), and the continuity of the far-field pattern (cf. Asms. 5.1 and 6.1). Asms. 2.1-3.4 are fulfilled in the two-dimensional case, and they are subject of future work for three dimensions. Asms. 5.1 and 6.1 should be verified by experiments. Suppose all assumptions are fulfilled and that the rough surface is a realization of random field. Then the smoothed far-field intensity function is the limit of smoothed intensity functions for periodized rough surfaces if the period tends to infinity. However, almost the same intensity function can be obtained with a fixed period by computing the average over many different realizations of the random field.

Finally, we report the numerical solution of a two-dimensional inverse problem (compare [40]), which is based on the intensity formula of our beam model. We assume that the rough surface is defined as a realization of a stationary, zero-mean, Gaussian random field with squared exponential kernel. Then, by means of a Bayesian inversion (cf. [23]), we infer the variance and the correlation length from measured scatterometric values. Naturally, these scatterometric values are the mean values of the intensities at a fixed direction. Additionally, we solve the problem by a Markov-chain Monte Carlo method (MCMC) (cf. [5]) with a surrogate model for the mapping from unknown parameters to intensities. This is done by a tensor-train approximation (cf. [28]). Note that such a method is expected to be efficient for rough surfaces with more involved random-field description.

The plan of the paper is as follows. In Sect. 2 we formulate the Dirichlet problem for the Helmholtz

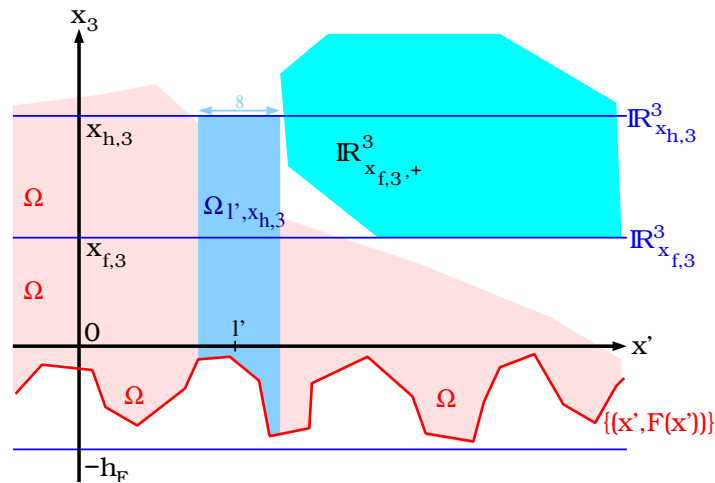


Figure 1: Geometry settings.

equation under plane-wave incidence in the half plane above a rough surface. We recall the classical formulae for the far field and the asymptotic intensity function. To approximate the solution by a boundary value problem over a finite domain, we approximate the surface by periodic or biperiodic surfaces in Sect. 3. For these grating structures, we describe the well-known solutions of diffraction and add the formula for the efficiencies, i.e., for the intensities of the reflected plane-wave modes. Sect. 4 contains the simple model of plane-wave beams of finite extent above gratings and the corresponding far-field asymptotics and intensity. In Sect. 5, we extend this model to the reflection by the rough surface leading to a diffuse scattering with a smooth far-field pattern, and in Sect. 6 we complement the model to deal with additional plane-wave beams in the directions of mirror reflection. A simple stochastic model for a rough surface represented as a random field is introduced in Sect. 7. For this, we present numerical simulations of the far-field intensities. In Sect. 8 we formulate an inverse problem for the reconstruction of the parameters of the random field from scatterometric data, i.e., from the mean values of measured intensities. The numerical solution by Bayesian inversion is proposed. Finally, in Sect. 9 we discuss a tensor-train surrogate model to improve the Bayesian inversion by an MCMC method.

2 Scattering by rough surfaces

In this section we shall introduce the deterministic notion of a rough surface. Later (cf. Sect. 7) each realization of a stochastic surface will be of this form. For the scattering of a plane wave by such a rough surface, we shall formulate the Dirichlet problem in the domain above the surface. Furthermore, we shall define the far-field pattern for the asymptotics of the wave solution in radial directions and add a formula for the asymptotic intensity distribution.

2.1 Boundary value problem and radiation condition

Throughout this paper we denote the points of the n -dimensional Euclidean space \mathbb{R}^n , $n=2,3$ by $\vec{x} := (x', x_3)^\top$ and $\vec{y} := (y', y_3)^\top$ with $x' := x_1$ for $n=2$ and $x' := (x_1, x_2)^\top \in \mathbb{R}^2$ for $n=3$. For fixed numbers $x_{f,n}$, we define the half spaces $\mathbb{R}^n_{x_{f,n},+} := \{(x', x_n)^\top \in \mathbb{R}^n : x_n > x_{f,n}\}$. The boundary planes take the form $\mathbb{R}^n_{x_{f,n}} := \{(x', x_{f,n})^\top : x' \in \mathbb{R}^{n-1}\}$. Furthermore, given a continuous function $F: \mathbb{R}^{n-1} \rightarrow \mathbb{R}$ such that $-h_F \leq F(x') < 0$ with fixed $h_F > 0$, our rough surface is the graph

$\Gamma_D := \{(x', F(x'))^\top : x' \in \mathbb{R}^{n-1}\}$ (cf. Fig. 1 for a two-dimensional sketch of the three-dimensional setting). We consider the half space $\Omega := \Omega_F := \{(x', x_n)^\top \in \mathbb{R}^n : x_n > F(x')\}$ above this surface Γ_D , and acoustic time-harmonic waves in Ω will be described by Helmholtz solutions $u : \Omega \rightarrow \mathbb{C}$, i.e., by solutions of $(\Delta + k^2 I)u = 0$ for a fixed wavenumber $k > 0$.

We assume that the Dirichlet problem of the Helmholtz equation over Ω has a unique solution, i.e., for a fixed wave number and for an incoming plane-wave function

$$\begin{aligned} u_{\text{inc}}(\vec{x}) &:= e^{i\vec{k}_{\text{inc}} \cdot \vec{x}}, \\ \vec{k}_{\text{inc}} = (k'_{\text{inc}}, k_{\text{inc},n})^\top &:= \begin{cases} k(\sin \theta_{\text{inc}}, -\cos \theta_{\text{inc}})^\top & \text{if } n=2 \\ k(\sin \theta_{\text{inc}} \cos \phi_{\text{inc}}, \sin \theta_{\text{inc}} \sin \phi_{\text{inc}}, -\cos \theta_{\text{inc}})^\top & \text{if } n=3 \end{cases} \end{aligned} \quad (2.1)$$

with incidence angles $-\frac{\pi}{2} < \theta_{\text{inc}} < \frac{\pi}{2}$ and $-\pi < \phi_{\text{inc}} < \pi$, there exists a unique scattered wave function u over Ω such that

$$\begin{aligned} \Delta u(\vec{x}) + k^2 u(\vec{x}) &= 0, \quad \vec{x} \in \Omega, \\ u((x', F(x'))^\top) &= -u_{\text{inc}}((x', F(x'))^\top), \quad x' \in \mathbb{R}^{n-1}, \\ u &\text{ satisfies the half-space radiation condition (HSRC).} \end{aligned} \quad (2.2)$$

Here we shall say that u satisfies the (HSRC) (cf. [31] and compare [11], [10], [9], [7], [13], [1, 21]) if there exist real numbers $c_u, \varepsilon_u, x_{h,n}$, and $x_{f,n}$ with $c_u > 0, \varepsilon_u > 0$, and $0 < x_{f,n} < x_{h,n}$ such that

- i) For any $l' \in \mathbb{Z}^{n-1}$, the restriction of u to $\Omega_{l', x_{h,n}} := \{\vec{x} \in \Omega : |x' - l'| < 4, x_n < x_{h,n}\}$ is in the Sobolev space $H^1(\Omega_{l', x_{h,n}})$ and has a bounded norm $\|u|_{\Omega_{l', x_{h,n}}}\|_{H^1(\Omega_{l', x_{h,n}})} < c_u$.
- ii) For the solution u with $n=2$ and for the second order derivative $\partial_{x_3}^2 u$ with $n=3$, there holds the representation

$$\begin{aligned} u(\vec{x}) &= 2 \int_{\mathbb{R}} \partial_{y_2} G_{2D}(\vec{x}, (y', x_{f,2})^\top) u((y', x_{f,2})^\top) dy', \quad \vec{x} \in \mathbb{R}_{x_{f,2},+}^2, \text{ and} \\ \partial_{x_3}^2 u(\vec{x}) &= 2 \int_{\mathbb{R}^2} \partial_{y_3}^3 G_{3D}(\vec{x}, (y', x_{f,3})^\top) u((y', x_{f,3})^\top) dy', \quad \vec{x} \in \mathbb{R}_{x_{f,3},+}^3, \end{aligned} \quad (2.3)$$

respectively. Here G_{nd} is the fundamental solution of the Helmholtz equation, i.e., this function is defined by $G_{3D}(\vec{x}, \vec{y}) := \frac{1}{4\pi} e^{ik|\vec{x}-\vec{y}|}/|\vec{x}-\vec{y}|$ for $n=3$ and $G_{2D}(\vec{x}, \vec{y}) := \frac{1}{4} H_0^{(1)}(k|\vec{x}-\vec{y}|)$ for $n=2$, respectively.

Concerning this definition, we note the following. The Dirichlet condition in (2.2) can be defined in the sense of traces for u satisfying item i) of the (HSRC). The four in the definition of $\Omega_{l', x_{h,n}}$ (cf. the diameter eight equal to two times four in Fig. 1) can be replaced by any sufficiently large number such that the surface Γ_D is completely covered by the $\Omega_{l', x_{h,n}}$, $l' \in \mathbb{Z}^{n-1}$. Item i) is a radiation condition in the sense that the asymptotic boundedness of $u(\vec{x})$ for $|\vec{x}| \rightarrow \infty$ along the rough surface is required. The uniform boundedness of $H^1(\Omega_{l', x_{h,n}})$ is natural since the setting of the rough surface is invariant w.r.t. shifts in the surface directions. Further, note that in well-known three-dimensional radiation conditions for wave functions decaying at infinity (upward propagating radiation condition), the field is represented as a double layer integral with the fundamental solution G_{3D} similarly to the two-dimensional case with G_{2D} . Differentiating this representation twice with respect to x_3 , we arrive at the weaker condition presented in item ii), which is defined for functions $u \in L^\infty(\mathbb{R}_{f,3}^3)$. Indeed, the

differentiated kernel takes the form

$$\begin{aligned} \partial_{y_3}^3 G_{3D}(\vec{x}, \vec{y}) = & \frac{e^{ik|\vec{x}-\vec{y}|}}{4\pi} \left\{ \frac{3(\mathbf{i}k)^2(y_3 - x_3)}{|\vec{x} - \vec{y}|^3} - \frac{9(\mathbf{i}k)(y_3 - x_3)}{|\vec{x} - \vec{y}|^4} + \frac{(\mathbf{i}k)^3(y_3 - x_3)^3}{|\vec{x} - \vec{y}|^4} \right. \\ & - \frac{6(\mathbf{i}k)^2(y_3 - x_3)^3}{|\vec{x} - \vec{y}|^5} + \frac{9(y_3 - x_3)}{|\vec{x} - \vec{y}|^5} + \frac{15(\mathbf{i}k)(y_3 - x_3)^3}{|\vec{x} - \vec{y}|^6} \\ & \left. - \frac{15(y_3 - x_3)^3}{|\vec{x} - \vec{y}|^7} \right\} = \mathcal{O}\left(\frac{1}{|x' - y'|^3}\right), \quad |x' - y'| \rightarrow \infty. \quad (2.4) \end{aligned}$$

Now we need

Assumption 2.1. Fix a special class Cl_{rs} of bounded continuous function over \mathbb{R}^{n-1} and consider the rough surfaces Γ_D , defined by functions $F \in Cl_{rs}$, together with the corresponding half spaces $\Omega = \Omega_F$ above Γ_D . We assume that, for any $F \in Cl_{rs}$ and for any incoming plane wave u_{inc} , there exists a unique solution of the scattering problem (2.2).

Remark 2.2. Existence and uniqueness for $n=2$ and for any continuous and uniformly bounded function F is shown in [7], where it is even proved that the solution belongs to a weighted Sobolev space. In other words, we can choose Cl_{rs} as the class of all continuous and bounded functions, and Asm. 2.1 is fulfilled. For the case $n=3$, such a result is not known and, probably, not true. We expect that future research will reveal the existence of special classes Cl_{rs} with Asm. 2.1.

2.2 Far field pattern, intensity, and measurement values

Next we turn to the far-field behaviour of the solution and to the measured intensity. To simplify notation, we consider the case $x_{f,n} = 0$, and we introduce the set $\mathbb{S}_+^{n-1} := \{\vec{x} \in \mathbb{R}^n : |\vec{x}| = 1, x_n > 0\}$ of directions pointing into the upper half space $\mathbb{R}_{0,+}^n$. We consider (2.3) and, for $n=3$, we assume for a moment that the representation of u by the double layer integral holds as well (i.e., the two-dimensional part in (2.3) with G_{2D} by G_{3D}), which is true for special $u((x', x_3)^\top)$ decaying for $|x'| \rightarrow \infty$. Taking the limit $r \rightarrow \infty$, we arrive at (cf. [12], Theorem 2.5)

$$\begin{aligned} u(r\vec{p}) &= 2 \int_{\mathbb{R}^{n-1}} \partial_{y_n} G(r\vec{p}, (y', 0)^\top) u((y', 0)^\top) dy', \quad \vec{p} = (p', p_3)^\top \in \mathbb{S}_+^{n-1}, \\ \lim_{r \rightarrow \infty} u(r\vec{p}) &= \frac{e^{ikr}}{r^{(n-1)/2}} \Phi(\vec{p}), \quad \Phi(\vec{p}) := C_n p_n [\mathcal{F}(u|_{\mathbb{R}_0^n})] \left(\frac{kp'}{2\pi} \right), \quad (2.5) \\ [\mathcal{F}f](\xi') &:= \int_{\mathbb{R}^{n-1}} e^{-i2\pi x' \cdot \xi'} f(x') dx', \quad C_n := \begin{cases} \frac{\sqrt{k}(1-i)}{2\sqrt{\pi}} & \text{if } n=2 \\ \frac{k}{2\pi i} & \text{if } n=3 \end{cases}. \end{aligned}$$

The function Φ is called far-field pattern. A similar asymptotics is well known from the far-field representation for the simpler case of scattering by bounded obstacles. For a general uniformly bounded $u|_{\mathbb{R}_0^3}$, we should replace (2.5) by

$$\lim_{r \rightarrow \infty} \partial_{x_3}^2 u(r\vec{p}) = \frac{e^{ikr}}{r} (\mathbf{i}kp_3)^2 \Phi(\vec{p}). \quad (2.6)$$

Indeed, setting $\vec{x} = r\vec{p}$, $y_3 = 0$ and replacing the differentiated kernel function $2\partial_{y_3}^3 G_{3D}(\vec{x}, \vec{y})$ in (2.3) by the expression $e^{ik|\vec{x}-\vec{y}|}(y_3 - x_3)^3|\vec{x} - \vec{y}|^{-4}$ (cf. the third term in (2.4)), we get

$$\begin{aligned} \frac{re^{-ikr}}{p_3^3} \int_{\mathbb{R}^2} e^{ik|\vec{x}-\vec{y}|} \frac{(y_3 - x_3)^3}{|\vec{x} - \vec{y}|^4} u(\vec{y}) \, dy' &= \int_{\mathbb{R}^2} u(\vec{y}) e^{-ikp' \cdot y'} \frac{e^{ik[|\vec{x}-\vec{y}| - |\vec{x}| + \vec{x} \cdot \vec{y}/r]} r^4}{|r\vec{p} - \vec{y}'|^4} \, dy' \\ &= \int_{\mathbb{R}^2} u(\vec{y}) e^{-ikp' \cdot y'} f(p', y', r) \, dy', \\ f(p', y', r) &:= \exp\left(ik \frac{|y'|^2 + (|rp' - y'| - r)p' \cdot y'}{|rp' - y'| + r}\right) \frac{r^4}{\sqrt{(rp' - y')^2 + r^2 p_3^2}^4}, \end{aligned}$$

where $f(p', y', r)$ on the right-hand side is uniformly bounded and tends to one for $r \rightarrow \infty$. In other words, for an absolutely integrable $u|_{\mathbb{R}_0^3}$, the integral tends to the Fourier transform of $u|_{\mathbb{R}_0^3}$ evaluated at $ky'/(2\pi)$ by Lebesgue's theorem on dominated convergence. We get (2.6) if we use the last derivation and similar formulae for $2\partial_{y_3}^3 G_{3D}(\vec{x}, \vec{y})$ in (2.3) replaced by the other terms (leading to asymptotic terms of lower order for $r \rightarrow \infty$) in the kernel representation (2.4).

In the case of a uniformly bounded smooth $u|_{\mathbb{R}_0^n}$, which does not decay at infinity, the above derivation breaks down since, for the application of Lebesgue's theorem, there is no integrable majorant function like $y' \mapsto C|u(\vec{y})|$ for the decaying case. However, we can approximate $u|_{\mathbb{R}_0^n}$ in the space of Schwartz distributions by decaying functions. Then the far-field pattern in (2.5) is the limit of the patterns corresponding to the far-fields of the waves defined by (2.3) with $u|_{\mathbb{R}_0^n} = u|_{\mathbb{R}_{x_{f,n}}^n}$ replaced by the approximate distributions of $u|_{\mathbb{R}_0^n}$. Clearly, in general the far-field pattern is a distribution. We expect that, in some sense, this far-field pattern is still a good model and useful to get measured scatterometric data in the subsequent Sect. 8. For the example of a plane wave $u_{pw}(\vec{x}) := \exp(i\vec{k}_{pw} \cdot \vec{x})$ with $|\vec{k}_{pw}| = k$ and $\vec{k}_{pw} = (k'_{pw}, k_{pw,n})^\top$, we obtain

$$\begin{aligned} \Phi_{pw}(\vec{p}) &:= \left[\frac{2\pi}{k}\right]^{n-1} C_n p_n \delta(p' - k'_{pw}/k) = \left[\frac{2\pi}{k}\right]^{n-1} C_n p_n \delta_{k'_{pw}/k}(p') \\ &= \left[\frac{2\pi}{k}\right]^{n-1} C_n \delta_{\vec{k}_{pw}/k}(\vec{p}) \end{aligned}$$

with the Dirac delta function δ . This corresponds to the peaks measured in the far-field at the propagation direction \vec{k}_{pw} . On the other hand, we have $u_{pw}(\vec{x} + r\vec{p}) = \exp(i\vec{k}_{pw} \cdot r\vec{p})u_{pw}(\vec{x})$, which tells us that there is no limit like in (2.5). With the exception of a complex factor of modulus one, the plane-wave field is everywhere the same. However, later we shall see the usefulness of the far-field notion (cf. (4.8)).

Now we switch to intensities. By arguments similar to (2.5) we conclude

$$\lim_{r \rightarrow \infty} [\nabla u](r\vec{p}) = \frac{e^{ikr}}{r^{(n-1)/2}} i\vec{k}\vec{p} \Phi(\vec{p}). \quad (2.7)$$

The intensity $\tilde{I}(\vec{x})$ is the average in time of the product of pressure and scaled velocity, i.e., the average in time of the product of $-\partial_t \Re e [u(\vec{x})e^{-i\omega t}]$ and $\frac{1}{\varrho_0} \nabla \Re e [u(\vec{x})e^{-i\omega t}]$ (cf. [12], Sect. 2.1 and note that ω is the frequency of the time-harmonic acoustic wave, ϱ_0 a fixed density value such that the true density of the medium is a function oscillating by a small amount about ϱ_0). For the far field, (2.5) and (2.7) imply

$$\begin{aligned} \tilde{I}(r\vec{p}) \cdot \vec{p} &= \frac{\omega k}{\varrho_0 r^{n-1}} \frac{1}{2\pi/\omega} \int_0^{2\pi/\omega} [\Re e \Phi(\vec{p}) \sin(kr - \omega t) + \Im m \Phi(\vec{p}) \cos(kr - \omega t)]^2 \, dt + o(1), \\ I(\vec{p}) &:= \lim_{r \rightarrow \infty} r^{n-1} \tilde{I}(r\vec{p}) \cdot \vec{p} = c_I |\Phi(\vec{p})|^2, \end{aligned} \quad (2.8)$$

where $c_I := k\omega^2/(2\rho_0)$ is a material constant.

Suppose the rough surface is irradiated by an inspecting laser beam modeled as a plane wave u_{inc} (cf. (2.1)). For a perfectly planar surface (i.e. $F = \text{const.}$), the reflected wave is $u_{\text{pw}}(\vec{x}) = e^{i\vec{k}\cdot\vec{x}}$ with $\vec{k} := k(\sin \theta_{\text{inc}}, \cos \theta_{\text{inc}})^\top$ and $\vec{k} := k(\sin \theta_{\text{inc}} \cos \phi_{\text{inc}}, \sin \theta_{\text{inc}} \sin \phi_{\text{inc}}, \cos \theta_{\text{inc}})^\top$, respectively. Of course, the case of a general F is more difficult. To measure the reflected wave for the general rough surface, a detector is placed in the reflection direction $\vec{k}/k \in \mathbb{S}^{n-1}$ of the perfect mirror at a distance d_1 . If this detector has an aperture diameter d_2 and if the angle ζ is defined as $\zeta := \arctan(d_2/(2d_1))$, then the vector \vec{p} points into the detector if and only if the angle between \vec{p} and \vec{k}/k is less than ζ , i.e., if and only if $\vec{p} \cdot [\vec{k}/k] > \cos \zeta$. Thus a simple model for a measured intensity is

$$I^{\text{meas}} = \int_{\{\vec{p} \in \mathbb{S}_+^{n-1} : \vec{p} \cdot [\vec{k}/k] > \cos \zeta\}} I(\vec{p}) \, d\vec{p}. \quad (2.9)$$

Depending on the properties of the detector an additional multiplicator for the intensity function in (2.9) is possible.

The asymptotic formulas (2.5), (2.7), and (2.8) are correct if the function $y' \mapsto u((y', 0)^\top)$ decays sufficiently fast for $|y'| \rightarrow \infty$. Unfortunately, in the general case the integral in (2.5) might not converge in the classical sense, and the Fourier transform $\mathcal{F}(u|_{\mathbb{R}_0^n})$ might be a distribution rather than a classical function. To get expressions with classical functions, we smoothen the far-field pattern. Roughly speaking, we replace the generalized function Φ by the smoothed function Φ_R , which is the convolution of $p' \mapsto \Phi((p', p_n)^\top)$ with a smooth function $p' \mapsto \hat{\psi}_R(p')$. Under the condition $\int_{\mathbb{R}^{n-1}} \hat{\psi}_R = 1$ and supposing that $\int_{p': |p'| > 1/R} \hat{\psi}_R$ is small, the smoothed function Φ_R is a smooth local average of Φ . Moreover, defining Φ_R for any positive R , the Φ_R tend to Φ for $R \rightarrow \infty$ in the distributional sense. Note that some kind of smoothing can be helpful to model the output data of the detection devices.

More precisely, we choose a three times continuously differentiable function $\psi > 0$ over \mathbb{R}^{n-1} such that $\psi(s') = 1$ for $|s'| \leq 1$ and $\psi(s') = 0$ for $|s'| \geq 2$ and denote the Fourier transform by $\hat{\psi} := \mathcal{F}\psi$. For a large $R > 0$, the dilated $\psi_R(s') := \psi(s'/R)$ has the transform $\hat{\psi}_R(p') := [\mathcal{F}\psi_R](p') = R^{n-1}\hat{\psi}(Rp')$ concentrated in a small neighbourhood of zero and with an integral $\int_{\mathbb{R}^{n-1}} \hat{\psi}_R = \psi_R(0) = 1$. The smoothed far-field pattern Φ_R is the convolution

$$\begin{aligned} \Phi_R(\vec{p}) &:= p_n(p') \int_{\mathbb{R}^{n-1}} \frac{1}{q_n(q')} \Phi((q', q_n(q'))^\top) \hat{\psi}_{Rk/2\pi}(p' - q') \, dq' \\ &= p_n(p') \left[\frac{\Phi((\cdot, q_n(\cdot))^\top)}{q_n(\cdot)} * \hat{\psi}_{Rk/2\pi} \right](p'), \\ p_n(p') &:= \sqrt{1 - |p'|^2}, \quad q_n(q') := \sqrt{1 - |q'|^2}, \end{aligned} \quad (2.10)$$

which rigorously can be defined as

$$\Phi_R(\vec{p}) := C_n p_n [\mathcal{F}(u|_{\mathbb{R}_0^n} \psi_R)] \left(\frac{kp'}{2\pi} \right), \quad \vec{p} = (p', p_n)^\top \in \mathbb{S}_+^{n-1}. \quad (2.11)$$

Note that this convolution corresponds to defining the far-field pattern in the distributional sense by the formulae $\langle \Phi_0, \varphi \rangle := C_n \int_{\mathbb{R}^2} u|_{\mathbb{R}_0^n} \mathcal{F}^{-1}\varphi$ and $\Phi(p', \sqrt{1 - |p'|^2}) = \sqrt{1 - |p'|^2} \Phi_0(kp'/2\pi)$. In this sense, Φ_R results from the smoothing of the distributional Φ_0 .

In accordance with (2.8) and (2.9), we define the smoothed far-field intensity $I_R(\vec{p}) := c_I |\Phi_R(\vec{p})|^2$ and the measured one by $I_R^{\text{meas}} = \int_{\{\vec{p} \in \mathbb{S}_+^{n-1} : \vec{p} \cdot [\vec{k}/k] > \cos \zeta\}} I_R(\vec{p}) \, d\vec{p}$.

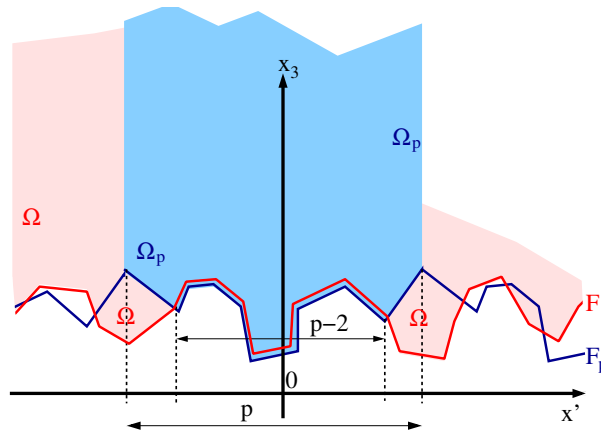


Figure 2: The periodized rough surface.

3 Periodic and biperiodic finite sections of the rough surface

In this section we introduce periodic and biperiodic finite sections of the rough surface Γ_D . Furthermore, we recall the definitions and results for the periodic and biperiodic solutions to the problem of scattered plane waves. We shall discuss far-field patterns and the asymptotics of the intensity.

Since a numerical simulation over an infinite domain is impossible, we shall restrict Ω to finite sections in horizontal direction, solve the corresponding Dirichlet problems together with lateral periodic and biperiodic boundary conditions, and consider periodic and biperiodic extensions of the solutions, respectively. More precisely, we choose a large period per (to avoid the overlapping of the subsequent periodization (3.1) at points of distance equal to $[\text{per } l']$, $l' \in \mathbb{Z}^{n-1}$, we suppose, at least, $\text{per} > 3$) and a smooth (at least continuous and s.t. the subsequent Asm. 3.1 holds) cut-off function χ defined on \mathbb{R} such that $\chi(t) = 1$ for $|t| \leq \frac{1}{2}$ and $\chi(t) = 0$ for $|t| \geq 1$. Then the function $\chi_{\text{per}}(t) := \chi(t + \text{per}/2)$ has its support around $\text{per}/2$. In the case $n=2$, we consider the per -periodic interval $[-\text{per}/2, \text{per}/2]$. To get a periodic approximation of F restricted to $[-\text{per}/2, \text{per}/2]$, we leave F unchanged in the interval $[-\text{per}/2, \text{per}/2 - 1]$ but change F close to $\text{per}/2$ such that the changed part fits periodically to the values of F close to $-\text{per}/2$. We add $\chi_{\text{per}}(x_1)[F(x_1 + \text{per}) - F(x_1)]$ to F , and the sum is smooth and per -periodic. In the case $n=3$, we apply a tensor-product transform of the case $n=2$. The resulting function

$$F_{\text{per}}(x') := \begin{cases} [1 - \chi_{\text{per}}(x_1)] F(x_1) + \chi_{\text{per}}(x_1) F(x_1 + \text{per}) & \text{if } n=2 \\ [1 - \chi_{\text{per}}(x_1)] [1 - \chi_{\text{per}}(x_2)] F(x') \\ + \chi_{\text{per}}(x_1) [1 - \chi_{\text{per}}(x_2)] F(x' + (\text{per}, 0)^\top) \\ + [1 - \chi_{\text{per}}(x_1)] \chi_{\text{per}}(x_2) F(x' + (0, \text{per})^\top) \\ + \chi_{\text{per}}(x_1) \chi_{\text{per}}(x_2) F(x' + (\text{per}, \text{per})^\top), & \text{if } n=3 \end{cases} \quad (3.1)$$

$$-\frac{\text{per}}{2} \leq x_j \leq \frac{\text{per}}{2}, \quad j = 1, \dots, n-1.$$

is equal to F for $-\text{per}/2 + 1 < x_j < \text{per}/2 - 1$, $j = 1, \dots, n-1$, and F_{per} admits a continuous periodic resp. biperiodic extension F_{per} to \mathbb{R}^{n-1} . The domain $\tilde{\Omega}_{\text{per}} := \Omega_{F_{\text{per}}}$ is defined as the perturbed half space over the periodic resp. biperiodic surface $\tilde{\Gamma}_{D,\text{per}} := \{\vec{x} \in \mathbb{R}^{n-1}: x_n = F_{\text{per}}(x')\}$. The finite section domain restricted to a single period of Ω is the column

$$\Omega_{\text{per}} := \left\{ \vec{x} \in \Omega_{F_{\text{per}}}: -\frac{\text{per}}{2} < x_j < \frac{\text{per}}{2}, \quad j = 1, \dots, n-1 \right\},$$

and the corresponding Dirichlet problem over this grating structure is (cf. Fig. 2)

$$\begin{aligned} \Delta u_{\text{per}}(\vec{x}) + k^2 u_{\text{per}}(\vec{x}) &= 0, \quad \vec{x} \in \tilde{\Omega}_{\text{per}}, \\ u_{\text{per}}(\vec{x} + (\text{per } l', 0)^\top) &= e^{i \text{per } k'_{\text{inc}} l'} u_{\text{per}}(\vec{x}), \quad \forall l' \in \mathbb{Z}^{n-1}, \quad \vec{x} \in \tilde{\Omega}_{\text{per}}, \\ u_{\text{per}}((x', F(x'))^\top) &= -u_{\text{inc}}((x', F(x'))^\top), \quad x' \in \mathbb{R}^{n-1}, \\ u_{\text{per}} &\text{ satisfies the half-space radiation condition (HSRC),} \end{aligned} \quad (3.2)$$

which, equivalently, can be considered over the column Ω_{per} only. Note that, for periodic resp. biperiodic structures condition (HSRC) is equivalent to the radiation condition for gratings. Namely, u_{per} satisfies (HSRC) if and only if it is the superposition of outgoing plane waves

$$\begin{aligned} u_{\text{per}}(\vec{x}) &= \sum_{l' \in \mathbb{Z}^{n-1}} c_{l'} e^{i \vec{\alpha}_{l'} \cdot \vec{x}}, \quad \forall \vec{x} \in \mathbb{R}^n, \quad x_n \geq 0, \\ \vec{\alpha}_{l'} &:= (\alpha'_{l'}, \alpha_{l',n})^\top, \quad \alpha'_{l'} := k'_{\text{inc}} + \frac{2\pi}{\text{per}} l', \quad \alpha_{l',n} := \begin{cases} \sqrt{k^2 - |\alpha'_{l'}|^2} & \text{if } k \geq |\alpha'_{l'}| \\ i \sqrt{|\alpha'_{l'}|^2 - k^2} & \text{else} \end{cases}, \end{aligned} \quad (3.3)$$

where $c_{l'}$ is a constant Rayleigh coefficient.

Assumption 3.1. We assume that together with F also the continuous functions $F_{\text{per}}: \mathbb{R}^{n-1} \rightarrow \mathbb{R}$ belong to the class Cl_{rs} of Asm. 2.1.

Remark 3.2. For $n=2$ and Cl_{rs} chosen as the class of uniformly bounded and continuous functions, Asm. 3.1 is satisfied.

Remark 3.3. Asm. 3.1 guarantees the existence of a unique solution to (3.2). Of course, unique solvability is known for the Dirichlet problem for any periodic and biperiodic surface Γ_{per} . However, if the Dirichlet boundary condition is switched to a different one, then this point should not be forgotten. Asm. 3.1 is also made to prepare the framework for Asm. 3.4.

Using (3.3) and (2.5), we conclude

$$\begin{aligned} [\mathcal{F}(u_{\text{per}}|_{\mathbb{R}_0^n})] &= \sum_{l' \in \mathbb{Z}^{n-1}} c_{l'} \delta_{\alpha'_{l'}/(2\pi)}, \quad [\mathcal{F}(u_{\text{per}}|_{\mathbb{R}_0^n})] \left(\frac{kp'}{2\pi} \right) = \left[\frac{2\pi}{k} \right]^{n-1} \sum_{l' \in \mathbb{Z}^{n-1}} c_{l'} \delta_{\alpha'_{l'}/k}(p'), \\ \Phi_{\text{per}}(\vec{p}) &= C_n \left[\frac{2\pi}{k} \right]^{n-1} p_n \sum_{l' \in \mathbb{Z}^{n-1}: |\alpha'_{l'}| \leq k} c_{l'} \delta_{\alpha'_{l'}/k}(p'), \\ \Phi_{\text{per},R}(\vec{p}) &= C_n \left[\frac{2\pi}{k} \right]^{n-1} p_n \sum_{l' \in \mathbb{Z}^{n-1}: |\alpha'_{l'}| \leq k} c_{l'} \hat{\psi}_{Rk/2\pi} \left(p' - \frac{\alpha'_{l'}}{k} \right), \quad \vec{p} = (p', p_n)^\top \in \mathbb{S}_+^2. \end{aligned} \quad (3.5)$$

Here, for the first identity, we have used the formula $\delta_{\alpha'_{l'}/(2\pi)}(k/2\pi \cdot) = [2\pi/k]^{n-1} \delta_{\alpha'_{l'}/k}$. Note that the far-field pattern Φ_{per} is defined by the second formula of (2.5), and an asymptotic relation for u_{per} similar to the first formula of (2.5) does not hold.

Now we look at the intensities. For a plane wave $u(\vec{x}) = e^{i \vec{\alpha} \cdot \vec{x}}$, we have the local intensity

$$\begin{aligned} \tilde{I}(\vec{x}, t) &= -\partial_t \Re [u(\vec{x}) e^{-i\omega t}] \frac{1}{\varrho_0} \nabla \Re [u(\vec{x}) e^{-i\omega t}] \\ &= \frac{\omega}{\varrho_0} \left\{ [\Re e^{i \vec{\alpha} \cdot \vec{x}}]^2 \sin^2(-\omega t) + [\Im e^{i \vec{\alpha} \cdot \vec{x}}]^2 \cos^2(-\omega t) \right. \\ &\quad \left. + 2[\Re e^{i \vec{\alpha} \cdot \vec{x}}][\Im e^{i \vec{\alpha} \cdot \vec{x}}] \sin(-\omega t) \cos(-\omega t) \right\} \vec{\alpha}. \end{aligned}$$

Taking time average, we arrive at

$$\tilde{I}(\vec{x}) = \frac{\omega}{2\varrho_0} |e^{i\vec{\alpha}\cdot\vec{x}}|^2 \vec{\alpha} = \frac{\omega}{2\varrho_0} \vec{\alpha}, \quad I(\vec{p}) = \frac{\omega k}{2\varrho_0} \left[\frac{\vec{\alpha}}{k} \right] \cdot \vec{p}. \quad (3.6)$$

No asymptotic limit $r \rightarrow \infty$ is needed.

For the superposition of two plane waves $u(\vec{x}) = ae^{i\vec{\alpha}\cdot\vec{x}} + be^{i\vec{\beta}\cdot\vec{x}}$ with complex valued coefficients, we analogously obtain

$$\begin{aligned} \tilde{I}(\vec{x}, t) &= \frac{\omega}{\varrho_0} \left\{ \Re [ae^{i\vec{\alpha}\cdot\vec{x}} + be^{i\vec{\beta}\cdot\vec{x}}] \sin(-\omega t) + \Im [ae^{i\vec{\alpha}\cdot\vec{x}} + be^{i\vec{\beta}\cdot\vec{x}}] \cos(-\omega t) \right\} \\ &\quad \times \left\{ \Re [ae^{i\vec{\alpha}\cdot\vec{x}} \vec{\alpha} + be^{i\vec{\beta}\cdot\vec{x}} \vec{\beta}] \sin(-\omega t) + \Im [ae^{i\vec{\alpha}\cdot\vec{x}} \vec{\alpha} + be^{i\vec{\beta}\cdot\vec{x}} \vec{\beta}] \cos(-\omega t) \right\}, \\ \tilde{I}(\vec{x}) &= \frac{\omega}{2\varrho_0} \left\{ \Re [ae^{i\vec{\alpha}\cdot\vec{x}} + be^{i\vec{\beta}\cdot\vec{x}}] \Re [ae^{i\vec{\alpha}\cdot\vec{x}} \vec{\alpha} + be^{i\vec{\beta}\cdot\vec{x}} \vec{\beta}] \right. \\ &\quad \left. + \Im [ae^{i\vec{\alpha}\cdot\vec{x}} + be^{i\vec{\beta}\cdot\vec{x}}] \Im [ae^{i\vec{\alpha}\cdot\vec{x}} \vec{\alpha} + be^{i\vec{\beta}\cdot\vec{x}} \vec{\beta}] \right\} \\ &= \frac{\omega}{2\varrho_0} \left\{ |a|^2 \vec{\alpha} + |b|^2 \vec{\beta} + \left[\Re (ae^{i\vec{\alpha}\cdot\vec{x}}) \Re (be^{i\vec{\beta}\cdot\vec{x}}) + \Im (ae^{i\vec{\alpha}\cdot\vec{x}}) \Im (be^{i\vec{\beta}\cdot\vec{x}}) \right] (\vec{\alpha} + \vec{\beta}) \right\}. \end{aligned}$$

Setting $a = |a|e^{ia_0}$ and $b = |b|e^{ib_0}$, we continue

$$\tilde{I}(\vec{x}) = \frac{\omega}{2\varrho_0} \left\{ |a|^2 \vec{\alpha} + |b|^2 \vec{\beta} + |a||b| \cos([\vec{\alpha} - \vec{\beta}] \cdot \vec{x} + a_0 - b_0) (\vec{\alpha} + \vec{\beta}) \right\}. \quad (3.7)$$

Clearly, for any open set $S \subset \mathbb{S}_+^{n-1}$ and for a difference $\vec{\alpha} - \vec{\beta}$ not in the closure of S , the parameter depending integral $\frac{1}{|rS|} \int_{rS} \cos([\vec{\alpha} - \vec{\beta}] \cdot \vec{x}) d\vec{x}$ is equal to the integral $\frac{1}{|S|} \int_S \cos(r[\vec{\alpha} - \vec{\beta}] \cdot [\vec{x}]) d\vec{x}$ and tends to zero for $r \rightarrow \infty$. Hence, in a weak limit (e.g. define the weak limit as the limit of averages $\lim_{r \rightarrow \infty} \frac{1}{\text{di}(r)} \int_r^{r+\text{di}(r)} \tilde{I}(\varrho \vec{p}) d\varrho$ with a fixed monotonically increasing diameter function di s.t. $\text{di}(r) \rightarrow \infty$ for $r \rightarrow \infty$) the coupling terms $|a||b| \cos([\vec{\alpha} - \vec{\beta}] \cdot \vec{x} + a_0 - b_0) (\vec{\alpha} + \vec{\beta})$ in Equ. (3.7) with $[\vec{\alpha} - \vec{\beta}] \cdot \vec{x} \neq 0$ can be neglected. We obtain, for $\vec{x} = r\vec{p}$ with $\vec{p} \in \mathbb{S}_+^{n-1}$ and $t \rightarrow \infty$, the far-field limit

$$\begin{aligned} I(\vec{p}) &:= \lim_{r \rightarrow \infty} \tilde{I}(r\vec{p}) \cdot \vec{p} \\ &= \begin{cases} \frac{\omega}{2\varrho_0} \left\{ |a|^2 \vec{\alpha} + |b|^2 \vec{\beta} \right\} \cdot \vec{p} & \text{if } \vec{p} \cdot [\vec{\alpha} - \vec{\beta}] \neq 0 \\ \frac{\omega}{2\varrho_0} \left\{ |a|^2 \vec{\alpha} + |b|^2 \vec{\beta} + \Re(a\bar{b}) (\vec{\alpha} + \vec{\beta}) \right\} \cdot \vec{p} & \\ = \frac{\omega}{2\varrho_0} |a + b|^2 \frac{\vec{\alpha} + \vec{\beta}}{2} \cdot \vec{p} & \text{else} \end{cases}. \end{aligned} \quad (3.8)$$

Now we observe that the plane wave functions $\vec{x} \mapsto e^{i\vec{\alpha}' \cdot \vec{x}}$ in (3.3) decay for large x_n if $|\alpha'_l| > k$. Thus in the asymptotics, we may restrict the sum in (3.3) to $l' \in \mathbb{Z}^2$ with $|\alpha'_{l'}| \leq k$. For the function u_{per} in (3.3), analogously to (3.8) we obtain the intensity formula

$$\begin{aligned} I_{\text{per}}(\vec{p}) &= \frac{\omega}{2\varrho_0} \left\{ \sum_{l' \in \mathbb{Z}^{n-1}: |\alpha'_{l'}| \leq k} |c_{l'}|^2 \vec{\alpha}_{l'} + \frac{1}{2} \sum_{\substack{l', m' \in \mathbb{Z}^{n-1}: l' \neq m', \\ |\alpha'_{l'}| \leq k, |\alpha'_{m'}| \leq k, \\ (\vec{\alpha}_{l'} - \vec{\alpha}_{m'}) \cdot \vec{p} = 0}} \Re(c_{l'} \bar{c}_{m'}) (\vec{\alpha}_{l'} + \vec{\alpha}_{m'}) \right\} \cdot \vec{p} \quad (3.9) \\ &= \frac{\omega}{2\varrho_0} \left\{ \alpha_{0',n} \sum_{l' \in \mathbb{Z}^{n-1}: |\alpha'_{l'}| \leq k} \frac{\vec{\alpha}_{l'} \cdot \vec{p}}{\alpha_{l',n}} E_{\text{per}, l'} + \frac{1}{2} \sum_{\substack{l', m' \in \mathbb{Z}^{n-1}: l' \neq m', \\ |\alpha'_{l'}| \leq k, |\alpha'_{m'}| \leq k, \\ (\vec{\alpha}_{l'} - \vec{\alpha}_{m'}) \cdot \vec{p} = 0}} \Re(c_{l'} \bar{c}_{m'}) (\vec{\alpha}_{l'} + \vec{\alpha}_{m'}) \cdot \vec{p} \right\}, \end{aligned}$$

where $0' = 0$ for $n=2$ and $0' = (0, 0)^\top$ for $n=3$, and where $E_{\text{per},l'}$ is the efficiency of the reflected plane wave mode $c_{l'} e^{i\vec{\alpha}_{l'} \cdot \vec{x}}$ of order $l' \in \mathbb{Z}^{n-1}$ with $|\alpha_{l'}'| \leq k$. This is given as (cf. e.g. Sect. 1.2.3 of [30])

$$E_{\text{per},l'} = \frac{\alpha_{l',n}}{\alpha_{0',n}} |c_{l'}|^2. \quad (3.10)$$

and is nothing else than the portion of energy over a unit time, which is radiated by the plane wave of propagation direction $\vec{\alpha}_{l'}$ through a unit area of a horizontal plane. Note that (3.9) is the correct formula if the distance of asymptotics r in $u(r\vec{p})$ is much larger than the wavelength but smaller than the lateral extent of the plane wave incidence.

Now we look at the convergence of the smoothed far-field patterns $\Phi_{\text{per},R}$ (cf. (2.11) and (3.5)) for $\text{per} \rightarrow \infty$. We expect that the solutions u_{per} of (3.2) converge to the solution u of (2.2) as $\text{per} \rightarrow \infty$. More precisely:

Assumption 3.4. *We suppose $F, F_{\text{per}} \in C^1_{\text{rs}}$ (cf. Asms. 2.1 and 3.1). For any fixed $l' \in \mathbb{Z}^{n-1}$ and the corresponding cylindrical domain $\Omega_{l',x_{h,n}}$, we assume that the solutions of (3.2) restricted to $\Omega_{l',x_{h,n}}$ converge to the solution of (2.2) restricted to $\Omega_{l',x_{h,n}}$ at least weakly in H^1 , i.e., for any $\varphi \in H^{-1}(\Omega_{l',x_{h,n}})$, there holds $\langle u_{\text{per}}|_{\Omega_{l',x_{h,n}}} - u|_{\Omega_{l',x_{h,n}}}, \varphi \rangle \rightarrow 0$ for $\text{per} \rightarrow \infty$.*

Remark 3.5. *Suppose $\text{per}_0 \geq 0$ is fixed and that, for any $\text{per} \geq \text{per}_0$ and any fixed $l' \in \mathbb{Z}^{n-1}$, the Sobolev norm $\|u_{\text{per}}\|_{H^1(\Omega_{l',x_{h,n}})}$ is bounded by a constant independent of per and l' , then Asm. 3.4 is satisfied.*

Remark 3.6. *For $n=2$, Asm. 3.4 follows similar to the results on non-periodic finite sections in weighted Sobolev spaces (cf. Sect. 5.2 of [7]).*

If we assume that Asm. 3.4 is true, then $u_{\text{per}}|_{\Omega_{l',x_{h,n}}}$ converges to $u|_{\Omega_{l',x_{h,n}}}$ strongly in $H^s(\Omega_{l',x_{h,n}})$ for $\text{per} \rightarrow \infty$, for any $0 \leq s < 1$, and for any $l' \in \mathbb{Z}^2$. Consequently, the analytic Helmholtz solutions u_{per} together with all their derivatives will converge on each compact subset of the line $\mathbb{R}^n_{x_{f,n}}$ with a last component $x_{f,n} > \sup_{x' \in \mathbb{R}^2} F(x')$ in the supremum norm. For a fixed R (cf. definition (2.11)) the smoothed far-field patterns $\Phi_{\text{per},R}$ are nothing else but the products of the function p_n multiplied by the Fourier transforms of the product $u_{\text{per}}\psi_R$ (cf. (2.11)), where ψ_R is a function of bounded support. Hence, for a fixed R and $\text{per} \rightarrow \infty$, the patterns $\Phi_{\text{per},R}$ together with all their derivatives converge to the pattern Φ_R and its derivatives in $L^\infty(\mathbb{S}_+^{n-1})$. Similarly, the far-field intensities $I_{\text{per},R} := c_I |\Phi_{\text{per},R}(\vec{p})|^2$ of the periodic resp. biperiodic finite sections will converge to the intensity I_R of the rough surface (cf. the end of Sect. 2.2).

We do not know, whether the I_{per} of the periodic structures converge to the I of the rough surface in some weak sense. To prove this by an argument based on formula (2.8) would require the square of a Dirac-delta, which is difficult to define.

4 Far-field beam model over periodized surfaces

In this section we replace the plane wave model of Sect. 3 by a simple model of beams with a finite cross section in the planes orthogonal to the direction of propagation. Though the waves are no solution of the Helmholtz equation at the boundary points of the beams, the far-field concept is more realistic than that for the plane waves. The shape of the cross section has no influence on the far-field.

Of course, real waves in the measurement settings are not plane waves over the full space. For example, in optical experiments with periodic gratings, we can see a light-beam of a diameter in the range

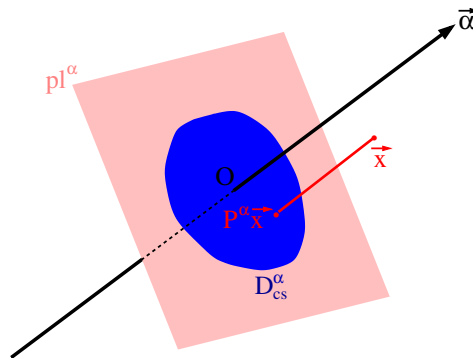


Figure 3: Cross-section domain D_{cs}^α of beam propagating in the direction of $\vec{\alpha}$. Domain D_{cs}^α is located in a plane perpendicular to $\vec{\alpha}$.

of a millimeter arriving onto the grating structure, and a finite number of similar light-beams appear as reflection. No scattering into other angular direction can be seen. Therefore, we model the plane waves as beams with a cross section close to an ellipsoidal domain (cf. Fig. 3 and the subsequent Eq. (4.1)), i.e., as a “plane wave with a finite diameter” (waist). In free space, the beams of the model propagate as rays. Close to the surface structure they are modeled by the rigorous diffraction theory of plane waves. However, the reflected plane waves leaving the surface are considered as beams again (cf. Fig. 4). Heuristically, this is acceptable since the beam diameter is in the millimeter range, which is huge in comparison to the wavelength or to the corrugations of the surface. We assume that the effect of a non-perfect model at the boundary of the rays can be neglected. In Fig. 4 the period has been increased. In pictures with the correct scaling of the rough surface the periodic corrugations are tiny in comparison to the beam diameter. Thus, in pictures, where the diameter of the beam is shown, the surface with small frequency corrugations would look like a planar surface (cf. the dotted line).

More precisely, suppose we have a plane wave $u_{pw}^\alpha(\vec{x}) := c_{pw} e^{i\vec{\alpha} \cdot \vec{x}}$ with $|\vec{\alpha}| = k$ and complex amplitude $c_{pw} \in \mathbb{C}$ propagating in the direction $\vec{\alpha}/k$, and suppose D_{cs}^α is a cross-section domain in the plane pl^α (cf. Fig. 3), which is normal to the direction and which contains the origin of the coordinate system. Here we assume that the origin is in the middle of the beam and at the rough surface. Obviously, the projection $P^\alpha \vec{x}$ of a vector \vec{x} onto the cross-section plane is $P^\alpha \vec{x} := \vec{x} - \frac{\vec{x} \cdot \vec{\alpha}}{\vec{\alpha} \cdot \vec{\alpha}} \vec{\alpha}$. We denote the characteristic function of D_{cs}^α over the plane by $\chi_{cs}^\alpha := \chi_{D_{cs}^\alpha}$ and model the beam of finite lateral extent by

$$u_{pw}^\alpha(\vec{x}) := c_{pw} e^{i\vec{\alpha} \cdot \vec{x}} \chi_{cs}^\alpha(P^\alpha \vec{x}) = c_{pw} e^{i\vec{\alpha} \cdot \vec{x}} \chi_{cs}^\alpha\left(\vec{x} - \frac{\vec{x} \cdot \vec{\alpha}}{\vec{\alpha} \cdot \vec{\alpha}} \vec{\alpha}\right). \quad (4.1)$$

This u_{pw}^α does not satisfy the Helmholtz equation at the boundary of the beam, i.e., at points \vec{x} with $P^\alpha \vec{x}$ at the boundary of the cross section D_{cs}^α .

Assumption 4.1. *The correct behaviour close to the lateral boundary of the beam can be neglected in the far-field behaviour.*

Remark 4.2. *This assumption is reasonable since the width of the beam is large in comparison to the wavelength, i.e., possible deviation of the wave in the distance less than a few wavelengths from the lateral boundary of the ray are not important in comparison to the plane-wave behaviour in regions, whose distance from the beam boundary is greater than a few wavelengths. Clearly, this argument is rigorous in the near field close to the surface, and the good approximation property of our simple model should be true up to a “certain distance” from the surface. This “certain distance” must be observed in experiments. In regions, where the beam cross section is nearly unchanged, the assumption of the*

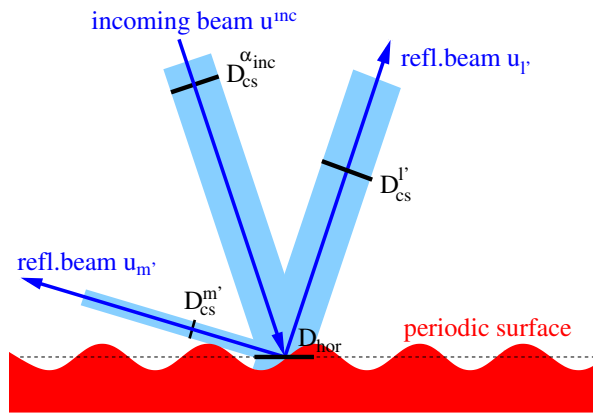


Figure 4: Wave as beams with ellipsoidal cross section of different diameters.

model is expected to be true, since any violation should result in a changed cross section. We assume that the measurement device is in the region of “certain distance”. Certainly, it is a big challenge to design measurement devices with good incident wave beams. On the other hand, the distance between measurement device and surface structure is in the range of something like twenty or more centimeters (wavelength in the range of visible light, beam diameter about a millimeter), which is huge in comparison to the beam width. So we really need the far-field behaviour of the beam with finite waist.

The solid angle, under which the cross section of the beam, perpendicular to the propagation, is seen from the origin, tends to zero if the cross section is moving along the propagation direction away from the origin. Consequently, the far-field intensity distribution (function depending on the directions originating at the origin) for the plane wave $u_{pw}^{\vec{\alpha}}$ of finite cross section $D_{cs}^{\vec{\alpha}}$ is approximately equal to a constant c_{ff} times the Dirac-delta function at $\vec{\alpha}/k \in \mathbb{S}_+^{n-1}$. Clearly, the constant c_{ff} is proportional to the measure $|D_{cs}^{\vec{\alpha}}|$ of the cross-section and to $|c_{pw}|^2$ (cf. the subsequent (4.4)).

Now suppose the incoming wave is a plane-wave beam with the exponent $\vec{\alpha} = \vec{\alpha}_{inc} = \vec{k}_{inc}$ and the cross section domain is $D_{cs}^{\vec{\alpha}} = D_{cs}^{\vec{\alpha}_{inc}}$. We suppose the periodic resp. biperiodic boundary surface $\tilde{\Gamma}_{D,per}$ is a perturbation of the plane $\mathbb{R}_0^n := \{\vec{x} \in \mathbb{R}^n : x_n = 0\}$ and denote the cross section of the ray in (4.1) with the horizontal plane \mathbb{R}_0^n by D_{ho} . As a simple model, we suppose the reflected plane waves in the representation for (3.3) are plane-wave beams defined by (4.1) with $\vec{\alpha} = \vec{\alpha}_{l'}$ (cf. (3.3)) and $D_{cs}^{\vec{\alpha}} = D_{cs}^{l'} := D_{cs}^{\vec{\alpha}_{l'}}$ such that the cross section of the ray with the horizontal plane \mathbb{R}_0^n is again D_{ho} . Then we get (cf. Fig. 4)

$$|D_{cs}^{\vec{\alpha}_{inc}}| = |D_{ho}| \frac{\alpha_{inc,n}}{k}, \quad |D_{cs}^{l'}| = |D_{ho}| \frac{\alpha_{l',n}}{k}, \quad |D_{cs}^{m'}| = |D_{cs}^{\vec{\alpha}_{inc}}| \frac{\alpha_{l',n}}{\alpha_{inc,n}}. \quad (4.2)$$

The function u_{per} , modified to propagating beams of finite diameters and with anything else neglected, is then given as

$$u_{per}^B(\vec{x}) := \sum_{l' \in \mathbb{Z}^{n-1} : |\alpha_{l'}| \leq k} c_{l'} e^{i\vec{\alpha}_{l'} \cdot \vec{x}} \chi_{cs}^{\vec{\alpha}_{l'}}(P^{\vec{\alpha}_{l'}} \vec{x}). \quad (4.3)$$

Using (3.6) and neglecting the modifications of the wave at the lateral boundary of the beam, the

intensity of the l' th reflected plane wave tested against the test function φ is

$$\begin{aligned}
\langle I_{l'}^B, \varphi \rangle &= \lim_{r \rightarrow \infty} \int_{r\mathbb{S}_+^{n-1}} |c_{l'}|^2 \frac{\omega}{2\rho_0} \vec{\alpha}_{l'} \cdot [\vec{x}/r] \chi_{\text{cs}}^{\vec{\alpha}_{l'}} \left(\vec{x} - \frac{\vec{x} \cdot \vec{\alpha}_{l'}}{\vec{\alpha}_{l'} \cdot \vec{\alpha}_{l'}} \vec{\alpha}_{l'} \right) \varphi(\vec{x}/r) d\vec{x} \\
&= |c_{l'}|^2 \frac{\omega}{2\rho_0} \lim_{r \rightarrow \infty} r^{n-1} \int_{\{\vec{x} \in \mathbb{S}_+^{n-1}: [\vec{x} - \frac{\vec{x} \cdot \vec{\alpha}_{l'}}{\vec{\alpha}_{l'} \cdot \vec{\alpha}_{l'}} \vec{\alpha}_{l'}] \in \frac{1}{r} D_{\text{cs}}^{l'}\}} \vec{\alpha}_{l'} \cdot \vec{x} \varphi(\vec{x}) d\vec{x} \\
&= |c_{l'}|^2 \frac{\omega k}{2\rho_0} |D_{\text{cs}}^{l'}| \varphi(\vec{\alpha}_{l'}/k), \\
I_{l'}^B &= |c_{l'}|^2 \frac{\omega k}{2\rho_0} |D_{\text{cs}}^{l'}| \delta_{\vec{\alpha}_{l'}/k} = \frac{\omega k}{2\rho_0} |D_{\text{cs}}^{\vec{\alpha}_{\text{inc}}}| \frac{\alpha_{l',n}}{\alpha_{\text{inc},n}} |c_{l'}|^2 \delta_{\vec{\alpha}_{l'}/k}. \tag{4.4}
\end{aligned}$$

Altogether, using $\alpha_{0l',n} = \alpha_{\text{inc},n}$ and recalling (3.10) and (4.2), we arrive at

$$\begin{aligned}
I_{\text{per}}^B(\vec{p}) &= \frac{\omega k}{2\rho_0} |D_{\text{cs}}^{\vec{\alpha}_{\text{inc}}}| \sum_{l' \in \mathbb{Z}^2: |\alpha_{l'}| \leq k} E_{\text{per},l'} \delta_{\vec{\alpha}_{l'}/k}(\vec{p}) = \sum_{l' \in \mathbb{Z}^2: |\alpha_{l'}| \leq k} E_{\text{per},l'} \delta_{\vec{\alpha}_{l'}/k}(\vec{p}) \tag{4.5} \\
&= p_n \sum_{l' \in \mathbb{Z}^2: |\alpha_{l'}| \leq k} E_{\text{per},l'} \delta_{\alpha_{l'}/k}(p').
\end{aligned}$$

Here, for the right-hand side of the first line, we assume the normalization that the average incoming energy $\int_{\mathbb{S}_+^{n-1}} I_{\text{inc}}^B(\vec{x}) d\vec{x} = \frac{\omega k}{2\rho_0} |D_{\text{cs}}^{\vec{\alpha}_{\text{inc}}}|$ is one s.t., due to energy conservation, the reflected energy is one as well, and the constant factor in front of the sum can be dropped. Applying such a normalization, there is no dependence on the cross section $D_{\text{cs}}^{\vec{\alpha}_{\text{inc}}}$ anymore.

At first glance, (4.5) seems to be the classical result of diffraction by periodic and biperiodic gratings, respectively. The portion of energy of the incoming wave radiated in the l' th reflected wave mode is the efficiency $E_{\text{per},l'}$. However, for the classical diffraction in Sect. 3, this is the time average of energy carried by the l' th wave mode over the units of any horizontal plane above the grating. Here, in the case of rays with finite diameter, it is the intensity (density function of energy flux depending on the directions in \mathbb{S}_+^2) irradiated into the space direction of the wave mode. By chance, the values for both energies coincide.

To get an asymptotic limit as a far-field pattern, the usual asymptotic factor $e^{ikr}/r^{(n-1)/2}$ (cf. (2.5)) is replaced by e^{ikr} . A simple calculation shows

$$\begin{aligned}
\langle \Phi_{\text{per}}^B, \varphi \rangle &:= \lim_{r \rightarrow \infty} \int_{r\mathbb{S}_+^{n-1}} e^{-ikr} \sum_{l' \in \mathbb{Z}^{n-1}: |\alpha_{l'}| \leq k} c_{l'} e^{i\vec{\alpha}_{l'} \cdot \vec{x}} \chi_{\text{cs}}^{\vec{\alpha}_{l'}} \left(\vec{x} - \frac{\vec{x} \cdot \vec{\alpha}_{l'}}{\vec{\alpha}_{l'} \cdot \vec{\alpha}_{l'}} \vec{\alpha}_{l'} \right) \varphi(\vec{x}/r) d\vec{x} \\
&= \sum_{l' \in \mathbb{Z}^{n-1}: |\alpha_{l'}| \leq k} c_{l'} |D_{\text{cs}}^{l'}| \varphi(\vec{\alpha}_{l'}/k), \tag{4.6} \\
\Phi_{\text{per}}^B(\vec{p}) &= \sum_{l' \in \mathbb{Z}^{n-1}: |\alpha_{l'}| \leq k} c_{l'} |D_{\text{cs}}^{l'}| \delta_{\vec{\alpha}_{l'}/k}(\vec{p}) = \frac{|D_{\text{cs}}^{\vec{\alpha}_{\text{inc}}}|}{\alpha_{\text{inc},n}} \sum_{l' \in \mathbb{Z}^{n-1}: |\alpha_{l'}| \leq k} c_{l'} \alpha_{l',n} \delta_{\vec{\alpha}_{l'}/k}(\vec{p}) \\
&= \frac{|D_{\text{cs}}^{\vec{\alpha}_{\text{inc}}}|}{\alpha_{\text{inc},n} k} \sum_{l' \in \mathbb{Z}^{n-1}: |\alpha_{l'}| \leq k} c_{l'} \alpha_{l',n}^2 \delta_{\alpha_{l'}/k}(p') = \frac{|D_{\text{cs}}^{\vec{\alpha}_{\text{inc}}}| p_n^2}{\alpha_{\text{inc},n}/k} \sum_{l' \in \mathbb{Z}^{n-1}: |\alpha_{l'}| \leq k} c_{l'} \delta_{\alpha_{l'}/k}(p'),
\end{aligned}$$

where, for the closed disc $\mathbb{D}^{n-1} := \{x' \in \mathbb{R}^{n-1} : |x'| < 1\}$ of radius one, we have used the integral transformation $\int_{\mathbb{S}_+^{n-1}} f(\vec{x}) \varphi(\vec{x}) d\vec{x} = \int_{\mathbb{D}_+^{n-1}} f(x', x_n) \varphi(x', x_n) \frac{1}{x_n} dx'$ with $x_n = \sqrt{1 - |x'|^2}$ s.t., for $f(\vec{x}) = \delta_{\vec{\alpha}_{l'}/k}(\vec{x})$, there holds

$$\int_{\mathbb{S}_+^{n-1}} \delta_{\vec{\alpha}_{l'}/k}(\vec{x}) \varphi(\vec{x}) d\vec{x} = \int_{\mathbb{D}_+^{n-1}} \frac{\alpha_{l',n-1}}{k} \delta_{\alpha_{l'}/k}(x') \varphi((x', x_n)^\top) \frac{1}{x_n} dx',$$

i.e., $\delta_{\alpha_{l'}/k}(\vec{x}) = [\alpha_{l',n}/k] \delta_{\alpha_{l'}/k}(x') = p_n \delta_{\alpha_{l'}/k}(x')$ with $p_n(p') := \sqrt{1 - |p'|^2}$. In the sense of (4.6) we get

$$u_{\text{per}}^B(r\vec{p}) = e^{ikr} \Phi_{\text{per}}^B(\vec{p}) + o(1), \quad r \rightarrow \infty, \quad (4.7)$$

$$\Phi_{\text{per}}^B(\vec{p}) := C_A p_n \sum_{l' \in \mathbb{Z}^{n-1}: |\alpha_{l'}| \leq k} c_{l'} \delta_{\alpha_{l'}/k}(\vec{p}) = C_A p_n^2 \sum_{l' \in \mathbb{Z}^{n-1}: |\alpha_{l'}| \leq k} c_{l'} \delta_{\alpha_{l'}/k}(p') \quad (4.8)$$

$$\vec{p} \in \mathbb{S}_+^{n-1}, \quad C_A := \frac{|D_{\text{CS}}^{\alpha_{\text{inc}}}|}{\alpha_{\text{inc},n}/k}.$$

Note that this far-field pattern $\Phi_{\text{per}}^B(\vec{p})$ is equal to the formally defined $\Phi_{\text{per}}(\vec{p})$ in (3.5) multiplied by the function p_n and by a constant factor. The additional factor p_n is clearly due to the introduction of a finite waist (cf. (4.2)). Again we define the smoothed far-field and the smoothed intensity (cf. (2.10) and (2.11)) by

$$\Phi_{\text{per},R}^B := p_n^2 \left(\frac{\Phi_{\text{per}}^B}{p_n^2} * \widehat{\psi}_{Rk/2\pi} \right) = C_A \left[\frac{k}{2\pi} \right]^{n-1} p_n^2 \left[\mathcal{F}(u_{\text{per}}|_{\mathbb{R}_0^n} \psi_R) \right] \left(\frac{kp'}{2\pi} \right), \quad (4.9)$$

$$I_{\text{per},R}^B(\vec{p}) := \frac{1}{C_A^2 [\alpha_{\text{inc},n}/k] p_n} |\Phi_{\text{per},R}^B|^2. \quad (4.10)$$

The factor $1/\{C_A^2 [\alpha_{\text{inc},n}/k] p_n\}$ in the last definition is borrowed from the subsequent Equ. (5.8). This choice and the arguments, following Asm. 3.4 and leading to $I_{\text{per},R} \rightarrow I_R$, imply $I_{\text{per},R}^B \rightarrow I_R^B$.

5 Far-field beam model for rough surface and its approximation

In this section we generalize the model of finite waist to the case of a rough surface. We suppose the incoming plane-wave beam is scattered by a rough surface and apply the same arguments and formulae as in Sect. 4.

Instead of a finite sum like in (3.3), we now have an integral

$$\begin{aligned} u((x', 0)^\top) &= \int_{\mathbb{R}^{n-1}} e^{i2\pi x' \cdot \xi'} [\mathcal{F}u|_{\mathbb{R}_0^n}](\xi') d\xi' \\ &= \int_{\mathbb{R}^{n-1}} \left[\frac{k}{2\pi} \right]^{n-1} [\mathcal{F}u|_{\mathbb{R}_0^n}]\left(\frac{kq'}{2\pi}\right) e^{ikq' \cdot x'} dq', \\ u(\vec{x}) &\approx \int_{\mathbb{S}_+^{n-1}} \left\{ \left[\frac{k}{2\pi} \right]^{n-1} [\mathcal{F}u|_{\mathbb{R}_0^n}]\left(\frac{kq'}{2\pi}\right) q_n \right\} e^{ik\vec{q} \cdot \vec{x}} d\vec{q}, \quad q_n := q_n(q') := \sqrt{1 - |q'|^2}, \end{aligned} \quad (5.1)$$

where we have used the radiation condition (angular spectrum representation, cf. [9]), which, for $n = 3$, is stronger than the (HSRC), and where the integral over the \vec{q} with $|q'| > 1$ are neglected.

Assumption 5.1. *We assume that the restriction of the function $q' \mapsto [\mathcal{F}(u|_{\mathbb{R}_0^n})](kq'/(2\pi)) q_n$ to the closed disc \mathbb{D}^{n-1} is continuous and that (5.1) provides a reasonable far-field approximation.*

Remark 5.2. *Note that the continuity condition on the Fourier transform $[\mathcal{F}u|_{\mathbb{R}_0^n}]$ is not fulfilled for all rough surfaces and all plane-wave reflections (cf. Sects. 4 and 5). It is just this condition, which leads to diffuse scattering in all directions with a continuous density function (cf. e.g. [26, Chapt. 7]). Consequently, Asm. 5.1 should be accepted for a special application if experiments confirm this.*

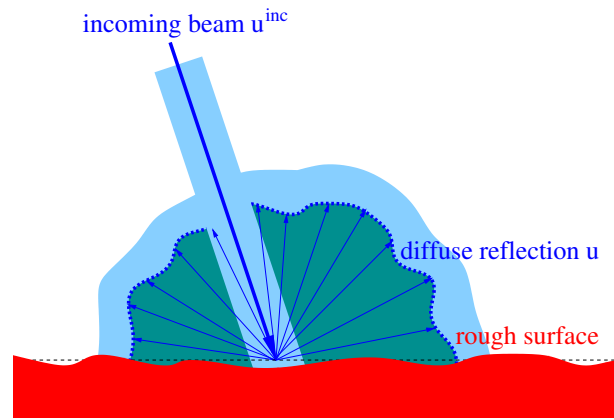


Figure 5: Diffuse scattering by rough surface. To make them visible, the lengths of the corrugations of the surface are increased.

Remark 5.3. Fix positive constants ε and c_j , $j=1, 2$. If the Fourier transform $\mathcal{F}(u|_{\mathbb{R}_0^n})$ can be estimated by $|\mathcal{F}(u|_{\mathbb{R}_0^n})(x')| \leq c_1 e^{-c_2|x'|^{1/2}}$ and if we consider the far field of $u(\vec{x})$ in the conical domain of all $\vec{x} = r\vec{p}$ such that $\vec{p} \in \mathbb{S}_{\varepsilon_D}^{n-1}$ with $\mathbb{S}_{\varepsilon_D}^{n-1} := \{\vec{p} \in \mathbb{S}_+^{n-1} : p_n \geq \varepsilon_D |p'|\}$, then the second part of Asm. 5.1 holds. Of course, the interesting case of grazing incidence (cf. e.g. [6] [36] [33]) with $|\theta_{\text{inc}}|$ close to $\pi/2$ is only covered at the price of larger constants.

Proof. The second part of Asm. 5.1 holds, i.e., the right-hand side of (5.1) is a good approximation, if the remainder integral

$$\int_{\mathbb{R}^{n-1} \setminus \mathbb{D}^{n-1}} \left[\frac{k}{2\pi} \right]^{n-1} [\mathcal{F}u|_{\mathbb{R}_0^n}]\left(\frac{kq'}{2\pi}\right) e^{ik\vec{q}\cdot\vec{x}} dq' \quad (5.2)$$

with $q := (q', q_n)^\top$ and $q_n := \mathbf{i}\sqrt{|q'|^2 - 1}$ is small. If we consider the far field of $u(\vec{x})$ in the conical domain, then the generalized plane wave $e^{ik\vec{q}\cdot\vec{x}}$ in (5.2) can be estimated as

$$\begin{aligned} |e^{ik\vec{q}\cdot\vec{x}}| &\leq e^{-kq_n x_n} \leq \begin{cases} e^{-kq_n \varepsilon_D |p'|r} \leq e^{-0.5 k \varepsilon_D q_n r} & \text{if } |p'| \geq 0.5 \\ e^{-kq_n p_n r} \leq e^{-\sqrt{0.75} k q_n r} & \text{if } |p'| = \sqrt{1 - p_n^2} \leq 0.5 \end{cases} , \\ &\leq e^{-c_E q_n r}, \quad c_E := k \min\{0.5 \varepsilon_D, \sqrt{0.75}\} , \end{aligned}$$

where $e^{-c_E q_n r}$ decays exponentially for $r \geq 1$ and $|q'| \rightarrow \infty$. Thus, if $q' \mapsto [\mathcal{F}(u|_{\mathbb{R}_0^n})](kq'/(2\pi))$ grows not faster than $e^{-c_E |q'|^{1/2}}$, then, by Lebesgue's theorem on dominated convergence, we conclude that the integral of (5.2) is small for large r . \square

Equation (5.1) corresponds to a diffuse scattering (cf. Fig. 5). In the far field, the plane wave $e^{ik\vec{x}\cdot\vec{q}}$ is replaced by the beam $e^{ik\vec{x}\cdot\vec{q}} \chi_{\text{cs}}^{\vec{q}}(\vec{x} - \frac{\vec{x}\cdot\vec{q}}{\vec{q}\cdot\vec{q}}\vec{q})$, i.e., by the wave (4.1) with $\vec{\alpha} = k\vec{q}$ and $D_{\text{cs}}^{\vec{\alpha}} = D_{\text{cs}}^{q'}$ such that the cross section of the ray with the horizontal plane \mathbb{R}_0^n is D_{ho} . Analogously to (4.3), we introduce

$$u(\vec{x}) \approx u^B(\vec{x}) := \int_{\mathbb{S}_+^{n-1}} \left\{ \left[\frac{k}{2\pi} \right]^{n-1} [\mathcal{F}u|_{\mathbb{R}_0^n}]\left(\frac{kq'}{2\pi}\right) q_n \right\} e^{ik\vec{x}\cdot\vec{q}} \chi_{\text{cs}}^{\vec{q}}\left(\vec{x} - \frac{\vec{x}\cdot\vec{q}}{\vec{q}\cdot\vec{q}}\vec{q}\right) d\vec{q}. \quad (5.3)$$

Instead of (4.4) derived for $c_{l'} e^{i\vec{\alpha}_{l'} \cdot \vec{x}} \chi_{cs}^{\vec{\alpha}_{l'}} \left(\vec{x} - \frac{\vec{x} \cdot \vec{\alpha}_{l'}}{\alpha_{l'}} \vec{\alpha}_{l'} \right)$, we get

$$\begin{aligned} \langle I_{\vec{q}}^B, \varphi \rangle &= \lim_{r \rightarrow \infty} \int_{r\mathbb{S}_+^{n-1}} \left| \left[\frac{k}{2\pi} \right]^{n-1} [\mathcal{F}u|_{\mathbb{R}_0^n}] \left(\frac{kq'}{2\pi} \right) q_n \right|^2 \frac{\omega k}{2\varrho_0} q' \cdot [\vec{x}/r] \chi_{cs}^{\vec{q}} \left(\vec{x} - \frac{\vec{x} \cdot \vec{q}}{\vec{q} \cdot \vec{q}} \vec{q} \right) \varphi(\vec{x}/r) d\vec{x} \\ &= \left| \left[\frac{k}{2\pi} \right]^{n-1} [\mathcal{F}u|_{\mathbb{R}_0^n}] \left(\frac{kq'}{2\pi} \right) q_n \right|^2 \frac{\omega k}{2\varrho_0} |D_{cs}^{\vec{q}}| \varphi(\vec{q}). \end{aligned} \quad (5.4)$$

Altogether, using $|D_{cs}^{\vec{q}}| = |D_{cs}^{\vec{\alpha}_{inc}}| k q_n / \alpha_{inc,n}$ (compare (4.2)), we arrive at

$$\begin{aligned} \langle I^B, \varphi \rangle &= \frac{\omega k^2}{2\varrho_0 \alpha_{inc,n}} |D_{cs}^{\vec{\alpha}_{inc}}| \int_{\mathbb{S}_+^{n-1}} \left| \left[\frac{k}{2\pi} \right]^{n-1} [\mathcal{F}u|_{\mathbb{R}_0^n}] \left(\frac{kq'}{2\pi} \right) q_n \right|^2 q_n \varphi(\vec{q}) d\vec{q}, \\ I^B(\vec{q}) &= \frac{\omega k^{2n} |D_{cs}^{\vec{\alpha}_{inc}}|}{2^{2n-1} \pi^{2n-2} \varrho_0 \alpha_{inc,n}} \left| [\mathcal{F}u|_{\mathbb{R}_0^n}] \left(\frac{kq'}{2\pi} \right) \right|^2 q_n^3 = C_I |\Phi(\vec{q})/C_n|^2 q_n \quad (5.5) \\ C_I &:= \left[\frac{k}{2\pi} \right]^{2(n-1)} \frac{1}{\alpha_{inc,n}/k}, \quad \Phi(\vec{q})/C_n = [\mathcal{F}u|_{\mathbb{R}_0^n}] \left(\frac{kq'}{2\pi} \right) q_n. \end{aligned}$$

Here, the same constant factor in front of the integral is dropped as in front of the sum in (4.5). Comparing (5.5) with (2.8), we see the same result except the different constant and except the additional factor q_n in (5.8). The last is due to the finite diameter of the beam (cf. (4.2)).

For the far-field pattern, a simple calculation shows

$$\begin{aligned} \langle \Phi^B, \varphi \rangle &:= \\ \lim_{r \rightarrow \infty} \int_{r\mathbb{S}_+^{n-1}} e^{-ikr} \int_{\mathbb{S}_+^{n-1}} \left\{ \left[\frac{k}{2\pi} \right]^{n-1} [\mathcal{F}u|_{\mathbb{R}_0^n}] \left(\frac{kq'}{2\pi} \right) q_n \right\} e^{ik\vec{q} \cdot \vec{x}} \chi_{cs}^{\vec{q}} \left(\vec{x} - \frac{\vec{x} \cdot \vec{q}}{\vec{q} \cdot \vec{q}} \vec{q} \right) d\vec{q} \varphi(\vec{x}/r) d\vec{x} \\ &= \int_{\mathbb{S}_+^{n-1}} \left[\frac{k}{2\pi} \right]^{n-1} [\mathcal{F}u|_{\mathbb{R}_0^n}] \left(\frac{kq'}{2\pi} \right) q_n |D_{cs}^{\vec{q}}| \varphi(\vec{q}) d\vec{q}, \\ \Phi^B(\vec{p}) &= C_B p_n^2 [\mathcal{F}u|_{\mathbb{R}_0^n}] \left(\frac{kp'}{2\pi} \right), \quad C_B := \left[\frac{k}{2\pi} \right]^{n-1} \frac{|D_{cs}^{\vec{\alpha}_{inc}}|}{\alpha_{inc,n}/k}, \quad (5.6) \end{aligned}$$

$$u^B(r\vec{p}) = e^{ikr} \Phi^B(\vec{p}) + o(1), \quad r \rightarrow \infty, \quad \vec{p} \in \mathbb{S}_+^{n-1}. \quad (5.7)$$

Note that $\Phi(\vec{p})$ in (2.5), multiplied by the function p_n and by a constant factor, is equal to $\Phi^B(\vec{p})$ in (5.6). From (5.5) we get

$$I^B(\vec{q}) = \frac{1}{C_A^2 [\alpha_{inc,n}/k] q_n} |\Phi^B(\vec{q})|^2. \quad (5.8)$$

Analogously to the smoothed far-field pattern Φ_R (cf. (2.11) and compare (4.9)), we define the convolution $\Phi_R^B(\vec{p}) := C_B p_n^2 [\mathcal{F}u|_{\mathbb{R}_0^n} \psi_R] \left(\frac{kp'}{2\pi} \right)$. Analogously to the smoothed far-field intensity function I_R (cf. (2.8) and the end of Sect. 2.2, compare (4.10)), we set $I_R^B(\vec{p}) := \frac{1}{C_A^2 [\alpha_{inc,n}/k] p_n} |\Phi_R^B(\vec{p})|^2$.

Collecting all the results, we arrive at

Theorem 5.4. *Suppose Asm. 2.1 is satisfied such that, in accordance with physics, there exist a unique wave solution of the scattering problem. Further suppose Asm. 4.1, i.e., that our beam model of finite extent is a good approximation. Observing, for our application in mind, a diffuse continuous far-field intensity function, we suppose Asm. 5.1. Then, for any given $\varepsilon > 0$, there is an $R_0 > 0$ such that,*

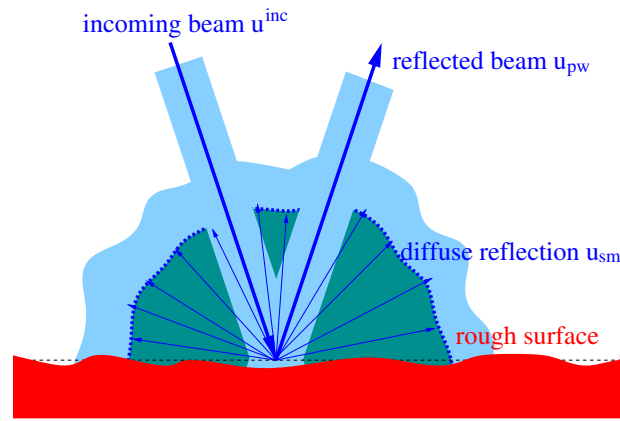


Figure 6: Reflected beam and diffuse scattering pattern for rough surface.

for any $R \geq R_0$, the supremum norm $\|I^B - I_R^B\|_{L^\infty}$ of the far-field intensities is less than ε . Finally, suppose the convergence of the periodized finite-section method in the sense of Asm. 3.4. Then there is a $\text{per}_0 = \text{per}_0(R_0) > 0$ such that, for any $\text{per} \geq \text{per}_0$, the supremum norm $\|I_{R_0}^B - I_{\text{per}, R_0}^B\|_{L^\infty}$ is less than ε , and $\|I^B - I_{\text{per}, R_0}^B\|_{L^\infty} \leq 2\varepsilon$.

Remark 5.5. Instead of an estimate with a small ε , a convergence rate can be derived. To get an estimate depending on R for the term $\|I^B - I_R^B\|_{L^\infty}$ an additional smoothness assumption for the function $\mathbb{D}^{n-1} \ni q' \mapsto [\mathcal{F}(u|_{\mathbb{R}_0^n})](kq'/(2\pi))$ is required. To estimate the deviation $\|I_{R_0}^B - I_{\text{per}, R_0}^B\|_{L^\infty}$ a convergence rate w.r.t. per for the finite section method is needed (cf. the rate for the non-periodic finite section method in [7]).

6 Scattering with additional plane-wave beam irradiated into the direction of the mirror reflection

Experimental observations show that, in the case of shallow roughness corrugations, the reflected field is the superposition of a beam propagating in the reflection direction of a perfect mirror plus a diffusely scattered wave (cf. Fig. 6 and the model presented in [32]). Therefore, we extend the scattering far-field of Sect. 5 in this section by an additional beam. Though, from the theoretical point of view, a representation without this beam and with a peak in the function u^B (cf. (5.3)) might be the correct approach, the additional plane-wave term will improve the approximation in numerical calculations.

The assumption and the precise notation of the above mentioned representation of the wave solution u are as follows (for the plausibility, compare Remarks 5.2 and 5.3).

Assumption 6.1. We assume $u = u_{pw} + u_{sm}$ is a reasonable far-field approximation with a plane wave $u_{pw}(\vec{x}) := c_{pw} e^{i\vec{\alpha}_{0'} \cdot \vec{x}}$ (cf. (3.4)) and with a wave u_{sm} of the form (5.1), where the restriction of the function $q' \mapsto [\mathcal{F}(u_{sm}|_{\mathbb{R}_0^n})](kq'/(2\pi))q_3$ to the closed disc \mathbb{D}^{n-1} is continuous.

For the modified field (cf. the terms in the sum of (3.3) and replace l' by $0'$, and cf. Fig. 6),

$$u^B = u_{pw}^B + u_{sm}^B, \quad u_{pw}^B(\vec{x}) := c_{pw} e^{i\vec{\alpha}_{0'} \cdot \vec{x}} \chi_{cs}^{\vec{\alpha}_{0'}} \left(\vec{x} - \frac{\vec{x} \cdot \vec{\alpha}_{0'}}{\vec{\alpha}_{0'} \cdot \vec{\alpha}_{0'}} \vec{\alpha}_{0'} \right). \quad (6.1)$$

Here the smooth part u_{sm}^B is a wave scattered diffusively by a finite part of the rough surface and can be treated like in (5.7) and (5.8). The plane-wave part can be treated like in (4.7) and (4.5).

In accordance with the representation (6.1), we get the splitting $\Phi^B = \Phi_{\text{pw}}^B + \Phi_{\text{sm}}^B$, where Φ_{pw}^B and Φ_{sm}^B are defined following (4.7) and (5.7), respectively. The intensity of the total field is the superposition of the intensities for the reflected plane-wave beam and that for the diffusively scattered wave (cf. (4.5) and (3.10) as well as (5.8)).

$$I^B = I_{\text{pw}}^B + I_{\text{sm}}^B, \quad I_{\text{pw}}^B(\vec{p}) := |c_{\text{pw}}|^2 \delta_{\vec{\alpha}_{0'}/k}(\vec{p}), \quad I_{\text{sm}}^B(\vec{p}) := \frac{1}{C_A^2[\alpha_{\text{inc},n}/k]p_n} |\Phi_{\text{sm}}^B(\vec{p})|^2, \quad (6.2)$$

Indeed, if we argue as in (4.4)-(4.5) and (5.4)-(5.5) and look at the limit for $r \rightarrow \infty$ of the integral of the smooth part of the intensity over the intersection of the tube

$$\left\{ \vec{x} \in \mathbb{R}^n : \chi_{\text{cs}}^{\alpha_{0'}} \left(\vec{x} - \frac{\vec{x} \cdot \vec{\alpha}_{0'}}{\vec{\alpha}_{0'} \cdot \vec{\alpha}_{0'}} \vec{\alpha}_{0'} \right) \neq 0 \right\}$$

in the direction $\vec{\alpha}_{0'}/k$ with the sphere of radius r , then the $\mathcal{O}(1/r)$ asymptotics of this diffusion part leads to no term of interaction at the mirror direction.

Now by u_{per}^B and Φ_{per}^B we denote the functions of (4.3) (cf. (3.2) and (3.3)) and (4.8) (cf. (3.5)), respectively. These are the functions corresponding to the periodized boundary and to the same plane-wave incidence as for the rough surface. Defining the smoothed patterns (compare Eqs. (2.10) and (2.11))

$$\begin{aligned} \Phi_{\text{per},R,\text{sm}}^B(\vec{p}) &:= p_n^2 \left[\frac{[\Phi_{\text{per}}^B - \Phi_{\text{pw}}^B](\cdot, q_n(\cdot))}{q_n^2(\cdot)} * \widehat{\psi}_{Rk/2\pi} \right](\vec{p}), \\ \Phi_{R,\text{sm}}^B(\vec{p}) &:= p_n^2 \left[\frac{\Phi_{\text{sm}}^B(\cdot, q_n(\cdot))}{q_n^2(\cdot)} * \widehat{\psi}_{Rk/2\pi} \right](\vec{p}) \end{aligned} \quad (6.3)$$

and using the supremum norm convergence of $u_{\text{per}}^B - u_{\text{pw}}^B$ to u_{sm}^B over bounded domains (cf. the arguments after Asm. 3.4), we obtain the convergence $\Phi_{\text{per},R,\text{sm}}^B \rightarrow \Phi_{R,\text{sm}}^B$ for $\text{per} \rightarrow \infty$ in any Sobolev norm (cf. the convergence $\Phi_{\text{per},R}^B \rightarrow \Phi_R^B$ at the end of Sect. 3). For large R , the pattern $\Phi_{R,\text{sm}}^B$ is close to the smooth pattern Φ_{sm}^B such that $\Phi_{\text{per},R,\text{sm}}^B$ is close to Φ_{sm}^B for large periods $\text{per} = \text{per}(R)$. Hence (cf. (6.2)), the intensity functions I_{sm}^B and I^B can be approximated by $I_{\text{per},R,\text{sm}}^B$ and $I_{\text{per},R}^B$, respectively.

$$\begin{aligned} I_{\text{per},R,\text{sm}}^B &:= \frac{1}{C_A^2[\alpha_{\text{inc},n}/k]p_n} |\Phi_{\text{per},R,\text{sm}}^B|^2, \quad I_{\text{per},R}^B := I_{\text{pw}}^B + \frac{1}{C_A^2[\alpha_{\text{inc},n}/k]p_n} |\Phi_{\text{per},R,\text{sm}}^B|^2, \\ I_{R,\text{sm}}^B &:= \frac{1}{C_A^2[\alpha_{\text{inc},n}/k]p_n} |\Phi_{R,\text{sm}}^B|^2. \end{aligned}$$

Recall that, for the rough surface with small corrugations (small amplitudes of the corrugations of function F), we experimentally observe that the scattered wave is a ray in the direction of the mirror reflection plus a wave scattered diffusively in all other direction (cf. the model in [32]). We assume that the corresponding intensity function is a continuous density. In accordance with this, for the periodic approximation, we split the Rayleigh coefficient $c_{0'}$ into $c_{0'} = c_{0',\text{pw}} + c_{0',\text{sm}}$. In the case of small corrugations, $c_{0',\text{pw}}$ should be a “small” perturbation of $c_{0'}$. The remainder value $c_{0',\text{sm}}$ is part of a diffuse reflection, i.e., $c_{0',\text{sm}}$ is the “smooth continuation” of the remaining reflection orders $c_{l',\text{sm}} := c_{l'}$ with $l' \neq 0'$. More precisely, we assume that, for large periods per , the $c_{l',\text{sm}}$ substituted into (4.8) lead to a smooth approximation of the regular far-field pattern Φ_{sm}^B , i.e., the pattern is $\Phi_{\text{per}}^B = \Phi_{\text{per},\text{pw}}^B + \Phi_{\text{per},\text{sm}}^B$ with (cf. (4.8))

$$\Phi_{\text{per},\text{pw}}^B := C_A p_n^2 (c_{0'} - c_{0',\text{sm}}) \delta_{\alpha_{0'}/k}, \quad \Phi_{\text{per},\text{sm}}^B := C_A p_n^2 \sum_{l' \in \mathbb{Z}^{n-1} : |\alpha_{l'}| \leq k} c_{l',\text{sm}} \delta_{\alpha_{l'}/k}. \quad (6.4)$$

The value $c_{0',\text{sm}}$ is chosen such that $\Phi_{\text{per,sm}}^B$ or, equivalently, $\frac{1}{p_n^2} \Phi_{\text{per,sm}}^B$ is a “nice” generalized function, i.e., the coefficients $c_{l',\text{sm}}$ of the uniformly distributed Dirac delta functions $\delta_{\alpha_{l'}/k}$ are the values of a smooth function restricted to the points $\alpha_{l'}/k$. The smoothing of such distributions by convolution with a smooth function of smaller support leads to smooth function with no spikes.

In view of (6.4) and

$$1 = \int \widehat{\psi}_{Rk/2\pi}(p' - q') dq' = \lim_{\text{per} \rightarrow \infty} \sum_{l' \in \mathbb{Z}^{n-1}} \widehat{\psi}_{Rk/2\pi}(p' - \alpha_{l'}/k) \left[\frac{2\pi}{k \text{ per}} \right]^{n-1}, \quad (6.5)$$

we get

$$\Phi_{\text{per},R,\text{sm}}^B \approx \Psi_{\text{per},R,\text{sm}}^B := C_A p_n^2 \frac{\sum_{l' \in \mathbb{Z}^{n-1} \setminus \{0'\}: |\alpha_{l'}| \leq k} c_{l',\text{sm}} \delta_{\alpha_{l'}/k} * \widehat{\psi}_{Rk/2\pi}}{\sum_{l' \in \mathbb{Z}^{n-1} \setminus \{0'\}: |\alpha_{l'}| \leq k} \left[\frac{2\pi}{k \text{ per}} \right]^{n-1} \delta_{\alpha_{l'}/k} * \widehat{\psi}_{Rk/2\pi}}. \quad (6.6)$$

By Equ. (6.4) and the definitions (4.9) and (6.3), we conclude

$$\begin{aligned} c_{0',\text{pw}} &= \frac{(c_{0'} - c_{0',\text{sm}}) \widehat{\psi}_{Rk/2\pi}(0')}{\widehat{\psi}_{Rk/2\pi}(0')} = \frac{\Phi_{\text{per},R,\text{pw}}^B(\alpha_{0'}/k)}{C_A [p_n(\alpha_{0'}/k)]^2 \widehat{\psi}_{Rk/2\pi}(0')} \\ &= \frac{\Phi_{\text{per},R}^B(\alpha_{0'}/k) - \Phi_{\text{per},R,\text{sm}}^B(\alpha_{0'}/k)}{C_A [p_n(\alpha_{0'}/k)]^2 \widehat{\psi}_{Rk/2\pi}(0')}, \\ c_{0',\text{pw}} &\approx c_{0',R,\text{pw}} := \frac{\Phi_{\text{per},R}^B(\alpha_{0'}/k) - \Psi_{\text{per},R,\text{sm}}^B(\alpha_{0'}/k)}{C_A [p_n(\alpha_{0'}/k)]^2 \widehat{\psi}_{Rk/2\pi}(0')}. \end{aligned} \quad (6.7)$$

Substituting (6.7), with $\Psi_{\text{per},R,\text{sm}}^B$ defined in (6.6), into the Φ_{pw}^B of Equ. (6.3) and replacing Φ_{sm}^B by $\Phi_{\text{per},R,\text{sm}}^B$ in (6.2), we arrive at the numerical approximation $I_{\text{per},R,\text{sm}}^B$ for I_{sm}^B .

Collecting all the results, we arrive at the following generalization of Thm. 5.4. Remark 5.5 holds in this case as well.

Theorem 6.2. *Suppose Asm. 2.1 is satisfied such that unique wave solutions are guaranteed for the scattering problem. Further suppose Asm. 4.1, i.e., that our beam model applies. To model a reflected beam in specular direction together with a diffuse continuous far-field intensity function, suppose Asm. 6.1. Then, for any given $\varepsilon > 0$, there is an $R_0 > 0$ such that, for any $R \geq R_0$, the supremum norm $\|\Phi_{\text{sm}}^B - \Phi_{R,\text{sm}}^B\|_{L^\infty}$ of the far-field patterns is less than ε . Finally, suppose the convergence of the periodized finite-section method in the sense of Asm. 3.4. Then there is a $\text{per}_0 = \text{per}_0(R_0) > 0$ such that, for any $\text{per} \geq \text{per}_0$, the supremum norm $\|I_{\text{sm}}^B - I_{\text{per},R_0,\text{sm}}^B\|_{L^\infty}$ as well as the deviation of the zeroth order Rayleigh coefficients $|c_{0',\text{pw}} - c_{0',R_0,\text{pw}}|$ are less than 2ε .*

On the other hand, we can also use a formula based on the efficiencies instead of the Rayleigh coefficients. For this we observe (cf. (6.3), (6.4), and (6.5)) that $\Phi_{\text{per},R,\text{sm}}^B$ is equal to p_n^2 times the quasi-interpolant of the complex values $\left[\frac{k \text{ per}}{2\pi} \right]^{n-1} c_{l',\text{sm}}$. Indeed,

$$\Phi_{\text{per},R,\text{sm}}^B(\vec{p}) = p_n^2 \sum_{l' \in \mathbb{Z}^{n-1}: |\alpha_{l'}| \leq k} \left[\frac{k \text{ per}}{2\pi} \right]^{n-1} c_{l',\text{sm}} \widehat{\psi}_{Rk/2\pi}(p' - \alpha_{l'}/k) \left[\frac{2\pi}{k \text{ per}} \right]^{n-1}, \quad (6.8)$$

where, for sufficiently large R , the function values of $\widehat{\psi}_{Rk/2\pi}(\cdot - \alpha'_{l'}/k)$ are concentrated in a small neighbourhood of $\alpha'_{l'}/k$. Of course, the approximation error of $\Phi_{\text{per},R,\text{sm}}^B$ by the quasi-interpolation is larger close to the boundary of \mathbb{D}^{n-1} , since the values at the interpolation points outside of \mathbb{D}^{n-1} are set to zero. However, the corresponding approximation error of Φ^B is improved due to multiplication by p_n^2 .

By the representation of $\Phi_{\text{per},R,\text{sm}}^B(\vec{p})$ as quasi-interpolant, the values $|\Phi_{\text{per},R,\text{sm}}^B(\vec{p})|^2$ can be approximated by p_n^4 times the quasi-interpolant of the values

$$\left[\frac{k \text{ per}}{2\pi}\right]^{2(n-1)} |c_{l',\text{sm}}|^2 = \left[\frac{k \text{ per}}{2\pi}\right]^{2(n-1)} \frac{\alpha_{0',n}}{\alpha_{l',n}} E_{\text{per},l',\text{sm}}, \quad l' \in \mathbb{Z}^{n-1} \text{ with } |\alpha_{l'}| \leq k, \quad (6.9)$$

$$E_{\text{per},l',\text{sm}} := \begin{cases} E_{\text{per},l'} = \frac{\alpha_{l',n}}{\alpha_{0',n}} |c_{l'}|^2 & \text{if } l' \neq 0' \\ |c_{0',\text{sm}}|^2 = \frac{\alpha_{0',n}}{\alpha_{0',n}} |c_{0',\text{sm}}|^2 & \text{if } l' = 0' \end{cases} \cdot \quad (6.10)$$

Here $E_{\text{per},0',\text{sm}} := |c_{0',\text{sm}}|^2$ is the efficiency of the difference wave of the $0'$ th order reflected wave in u_{per} (cf. (3.3)) minus the wave u_{pw} . Surely, the quasi-interpolant of $|\Phi_{\text{per},R,\text{sm}}^B(\vec{p})|^2$ can be replaced by an average value of all the numbers in (6.9) with l' , for which $\alpha_{l'}/k \in \mathbb{D}_+^{n-1}$ is close to p' .

Recall that, for the rough surface with small corrugations (small amplitudes of the corrugations of function F), we experimentally observe that the scattered wave is a ray in the direction of the mirror reflection plus a wave scattered diffusively in all other direction (cf. the model in [32]). We assume that the corresponding intensity function is a continuous density. In accordance with this, for the periodic approximation, we split $E_{\text{per},0'}$ into $E_{\text{per},0'} = E_{\text{per},\text{pw}} + E_{\text{per},0',\text{sm}}$, where $E_{\text{per},\text{pw}}$ is the energy portion transmitted by an approximate plane-wave reflection. In the case of small corrugations, this should be a “small” perturbation of $E_{\text{per},0'}$. The remainder value $E_{\text{per},0',\text{sm}}$ is part of a diffuse reflection, i.e., $E_{\text{per},0',\text{sm}}$ is the “smooth continuation” of the remaining reflection orders $E_{\text{per},l'}$ with $l' \neq 0'$. More precisely, we assume that, for large periods per , the $E_{\text{per},l',\text{sm}}$ substituted into (4.5) lead to a smooth approximation of the regular intensity distribution I_{sm}^B , i.e, the total intensity is $I_{\text{per}}^B = I_{\text{per},\text{pw}}^B + I_{\text{per},\text{sm}}^B$ with (cf. (4.5))

$$\begin{aligned} I_{\text{per},\text{pw}}^B &:= (E_{\text{per},0'} - E_{\text{per},0',\text{sm}}) \delta_{\vec{\alpha}_{0'}/k}, & I_{\text{per},\text{sm}}^B &:= \sum_{l' \in \mathbb{Z}^{n-1}: |\alpha_{l'}| \leq k} E_{\text{per},l',\text{sm}} \delta_{\vec{\alpha}_{l'}/k} \\ & & &:= p_n \sum_{l' \in \mathbb{Z}^{n-1}: |\alpha_{l'}| \leq k} E_{\text{per},l',\text{sm}} \delta_{\alpha_{l'}/k}. \end{aligned}$$

The value $E_{\text{per},0,\text{sm}}$ with $0 \leq E_{\text{per},0,\text{sm}} \leq E_{\text{per},0}$ is chosen such that $I_{\text{per},\text{sm}}^B$ or, equivalently, $\frac{1}{p_n} I_{\text{per},\text{sm}}^B$ is a “nice” generalized function (compare the “nice” function $\frac{1}{p_n^2} \Phi_{\text{per},\text{sm}}^B$). In view of (6.2), (6.8), and

(6.5), we get

$$\begin{aligned} \frac{1}{p_n} I_{\text{per},R,\text{sm}}^B &:= \frac{\sum_{l' \in \mathbb{Z}^{n-1} \setminus \{0'\}: |\alpha'_{l'}| \leq k} E_{\text{per},l',\text{sm}} \delta_{\alpha'_{l'}} * \widehat{\psi}_{Rk/2\pi}}{\sum_{l' \in \mathbb{Z}^{n-1} \setminus \{0'\}: |\alpha'_{l'}| \leq k} \left[\frac{2\pi}{k \text{ per}} \right]^{n-1} \delta_{\alpha'_{l'}} * \widehat{\psi}_{Rk/2\pi}} \\ &\approx \left[\frac{1}{q_n(\cdot)} I_{\text{per},\text{sm}}^B \right] * \widehat{\psi}_{Rk/2\pi}, \end{aligned} \quad (6.11)$$

$$\left[\frac{2\pi}{k \text{ per}} \right]^{n-1} \frac{1}{p_n} I_{\text{per},R,\text{sm}}^B(\vec{p}) = E_{\text{per},R,\text{sm}}^B(p'), \quad \vec{p} = (p', p_n)^\top \in \mathbb{S}_+^2, \quad (6.12)$$

$$E_{\text{per},R,\text{sm}}^B(p') := \frac{\sum_{l' \in \mathbb{Z}^{n-1} \setminus \{0'\}: |\alpha'_{l'}| \leq k} E_{\text{per},l',\text{sm}} \widehat{\psi}_{Rk/2\pi} \left(p' - \frac{\alpha'_{l'}}{k} \right) \left[\frac{2\pi}{k \text{ per}} \right]^{n-1}}{\sum_{l' \in \mathbb{Z}^{n-1} \setminus \{0'\}: |\alpha'_{l'}| \leq k} \widehat{\psi}_{Rk/2\pi} \left(p' - \frac{\alpha'_{l'}}{k} \right) \left[\frac{2\pi}{k \text{ per}} \right]^{n-1}}. \quad (6.13)$$

Here $E_{\text{per},R,\text{sm}}^B(p')$ is a quasi-interpolation of the values $E_{\text{per},l',\text{sm}}^B$ such that $E_{\text{per},R,\text{sm}}^B(\alpha'_{0'}/k)$ approximates $E_{\text{per},0',\text{sm}}$, which is equal to $[E_{\text{per},0'} - E_{\text{per},\text{pw}}]$. For $E_{\text{per},\text{pw}}$, we arrive at the approximation

$$E_{\text{per},R,\text{pw}} := E_{\text{per},0'} - E_{\text{per},R,\text{sm}}^B \left(\frac{\alpha'_{0'}}{k} \right). \quad (6.14)$$

For the measured intensity in (2.9) with I replaced by I^B , we get the approximation

$$\begin{aligned} I_{\text{per},R}^{\text{meas}} &:= E_{\text{per},R,\text{pw}} + \int_{\{\vec{p} \in \mathbb{S}_+^2: \vec{p} \cdot [\vec{\alpha}'_{0'}/k] > \cos \zeta\}} I_{\text{per},R,\text{sm}}^B(\vec{p}) \, d\vec{p} \\ &\approx E_{\text{per},R,\text{pw}} + \pi \tan^2(\zeta) I_{\text{per},R,\text{sm}}^B \left(\frac{\vec{\alpha}'_{0'}}{k} \right) \\ &= E_{\text{per},R,\text{pw}} + \pi \tan^2(\zeta) \left[\frac{k \text{ per}}{2\pi} \right]^{n-1} \frac{\alpha'_{0',n}}{k} E_{\text{per},R,\text{sm}}^B \left(\frac{\alpha'_{0'}}{k} \right). \end{aligned} \quad (6.15)$$

The formulae (6.13), (6.14), and (6.15) provide us a way to simulate the measured values from solving the boundary value problem above the periodized surface.

7 Stochastic simulation of gratings with rough surfaces

In this section we describe how to construct gratings with stochastic surfaces. Each of this can be considered as a periodization of a non-periodic rough surface structure. So we can compute the smoothed intensities of these gratings and consider them as approximations of non-periodic rough surfaces. We can study the mean values of these entities, which provide us the simulated measurement data for the inverse problem of Sect. 8. In any case, we restrict our consideration to the simplest model.

In comparison with $-h_F \leq F(x') < 0$ required in Sect. 2.1, we now shift the coordinates of the rough surface in x_n direction such that the coordinate x_n is zero for the points of the ideal planar surface without roughness and such that $F(x')$ is fluctuating around zero. To get a grating with rough interface, we define the interface height $F(x')$ depending on x' as a realization of a stochastic field. We consider the model

- i) Suppose that $F_{\text{per}}: \mathbb{R}^{n-1} \rightarrow \mathbb{R}$ is periodic for $n=2$ and biperiodic for $n=3$ with the periods equal to per .
- ii) For each $x' \in \mathbb{R}^2$, we assume that $F_{\text{per}}(x')$ is a random variable $\omega \mapsto F_{\text{per}}(x', \omega)$ with mean value $\mathbf{E}[F_{\text{per}}(x')] = 0$ and standard deviation $\hat{s} := \sqrt{\mathbf{E}[(F_{\text{per}}(x') - 0)^2]}$ independent of x' .
- iii) For each $x', y' \in \mathbb{R}^2$, we assume that the random variables $F(x')$ and $F(y')$ are correlated such that $\text{corr}(F(x'), F(y')) := \mathbf{E}[(F(x') - 0)(F(y') - 0)]/\hat{s}^2 = e^{-|x' - y'|_*^2/\hat{l}^2}$ with the periodized Euclidean distance $|x' - y'|_* := \min\{|x' - y' + \text{per } l'| : l' \in \mathbb{Z}^{n-1}\}$ and with the correlation length \hat{l} independent of x' and y' .

The correlation function $(x', y') \mapsto \text{corr}(F(x'), F(y'))$ is the Fourier transform of the power spectral density, the standard deviation \hat{s} is the root mean square height, and the reciprocal correlation length $1/\hat{l}$ determines the frequency level of the corrugations due to roughness (cf. [13]). Equivalently to i)-iii), by the Karhunen-Loève expansion (compare the representation of coefficients for stochastic partial differential equations in [4]), we get the representation

$$F(x', \omega) = \hat{s} \sum_{m' \in \mathbb{Z}^{n-1}: m_j \geq 0}^{\infty} \sqrt{\lambda_{m'}} \sum_{m_0=1}^{2(n-1)} Y_{m', m_0}(\omega) \varphi_{m', m_0}^{\text{corr}}(x'), \quad (7.1)$$

where, by $Y_{m', m_0}(\omega)$, we denote independent normally distributed random numbers with mean value zero and standard deviation one. The convergence holds in the L^2 norm w.r.t. the random variable ω (even almost surely) and uniformly w.r.t. x' . The values $\lambda_{m'}$ and the functions $\varphi_{m', m_0}^{\text{corr}}$ with $1 \leq m_0 \leq 2(n-1)$ in (7.1) are the eigenvalues and the eigenfunctions of the integral operator over the periodic domain $[0, \text{per}]^{n-1}$ with correlation kernel $k(x', y') = e^{-|x' - y'|_*^2/\hat{l}^2}$. The eigenfunctions $\varphi_{m_1, m_0}^{\text{corr}}$ for $n=2$ and $\varphi_{m', m_0}^{\text{corr}}$ for $n=3$, respectively, of the operator with a general correlation kernel $k(x', y') = \text{corr}(F(x'), F(y')) = \text{cor}(|x' - y'|_*)$ are given by

$$\begin{aligned} \varphi_{m_1, m_0}^{\text{corr}}(x_1) &:= \sqrt{\frac{2\pi}{\text{per}}} \begin{cases} \cos\left(\frac{2\pi}{\text{per}} x_1\right) & \text{if } m_0 = 1 \\ \sin\left(\frac{2\pi}{\text{per}} x_1\right) & \text{if } m_0 = 2 \end{cases}, \\ \varphi_{m', 2(j_1-1)+j_2}^{\text{corr}}(x') &:= \varphi_{m_1, j_1}^{\text{corr}}(x_1) \varphi_{m_2, j_2}^{\text{corr}}(x_2), \quad j_1, j_2 = 1, 2. \end{aligned}$$

The corresponding eigenvalues of this convolution operator are the Fourier coefficients

$$\lambda_{m'} := \begin{cases} \int_{-\text{per}/2}^{\text{per}/2} \text{cor}(|z_1|_*) e^{iz_1 m_1} dz_1 & \text{if } n = 2 \\ \int_{-\text{per}/2}^{\text{per}/2} \int_{-\text{per}/2}^{\text{per}/2} \text{cor}(|z'|_*) e^{iz' \cdot m'} dz_2 dz_1 & \text{if } n = 3. \end{cases}$$

In particular, for $k(x', y') = e^{-|x' - y'|_*^2/\hat{l}^2}$, we get

$$\begin{aligned} \lambda_{m'} &:= \prod_{j=1}^{n-1} \lambda_{m_j}, \quad \lambda_{m_j} := \int_{-\text{per}/2}^{\text{per}/2} e^{-t^2/\hat{l}^2} e^{itm_j} dt = 2 \int_0^{\text{per}/2} e^{-t^2/\hat{l}^2} \cos(tm_j) dt \\ &= \frac{\sqrt{\pi}}{4} \hat{l} e^{-[\hat{l}m_j]^2/4} + \mathcal{O}\left(\frac{e^{-[\text{per}/\hat{l}]^2/8}}{[\text{per}/\hat{l}]}\right), \quad \text{per} \rightarrow \infty. \end{aligned}$$

In our numerical computations we consider the case $n=2$ only. For simplicity and for easier implementation, we replace the normally distributed Y_{m', m_0} by uniformly distributed random numbers,

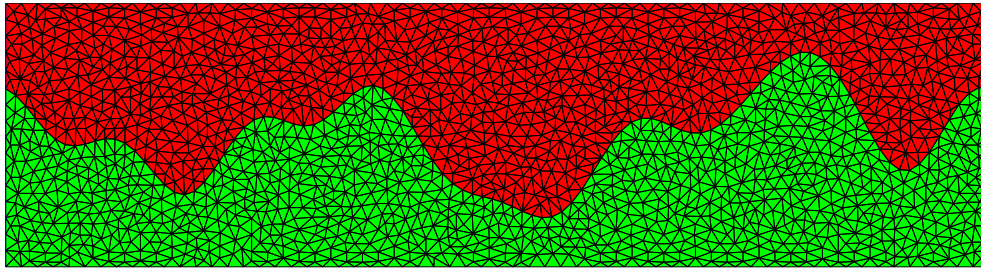


Figure 7: Example of rough periodic 2D grating.

though not all fields with uniformly distributed $F(x')$ (cf. condition ii)) can be represented by the (7.1) with independent Y_{m',m_0} . Furthermore, we restrict the infinite sum to a sum over $M=16$ terms. Finally, we replace the correlation function with the eigenvalues $\lambda_{m'}$ by a similar one with the simpler eigenvalues a_m^2 . Altogether, for the $x_1 = x' \in \mathbb{R}^{n-1}$, we use the representation

$$F(x', \omega) = \hat{s} \sum_{m=1}^M a_m \left\{ \sin\left(m \frac{2\pi}{\text{per}} x'\right) Y_{2m}(\omega) + \cos\left(m \frac{2\pi}{\text{per}} x'\right) Y_{2m+1}(\omega) \right\}, \quad (7.2)$$

$$a_m := \frac{e^{-m^2 \hat{l}^2 / 2}}{\sqrt{\sum_{n=1}^{16} e^{-n^2 \hat{l}^2}}},$$

with independent random numbers $Y_m(\omega)$ uniformly distributed in $(-1, 1)$. A realization of (7.2) over a period of $\text{per} = 8 \mu\text{m}$ with standard deviation $\hat{s} = 0.25 \mu\text{m}$ and correlation length $\hat{l} = 0.125 \mu\text{m}$ is shown in Fig. 7.

The Dirichlet boundary condition at the rough surface in the preceding sections has been chosen since this is the condition with the best theoretical results. For the numerical experiments it is not essential. We only have to suppose that our assumptions on the solutions are satisfied, that the unique solvability is guaranteed, and that the periodized finite section converges. So we use a more practical boundary condition in our computations, i.e., we consider a TE-polarized electro-magnetic wave, air as cover material above the rough surface, and silicon as substrate material below. This means that the Dirichlet condition is replaced by continuous transmission conditions for u and for its normal derivative over the rough surface. A second radiation condition for u in the lower half space is added.

Next we consider irradiation from above, i.e., the reflection u of an incoming plane wave with incidence angle $\theta_{\text{inc}} = 0^\circ$ such that $k'_{\text{inc}} = \alpha'_{0'} = 0$ (cf. (2.1) and (3.4)). We irradiate a single rough surface of period $\text{per} = 128 \mu\text{m}$, with a standard deviation of the heights $F(x_1)$ equal to $\hat{s} = 0.25 \mu\text{m}$, and with correlation length $\hat{l} = 0.50 \mu\text{m}$ by a plane wave beam of wavelength $\lambda = 400 \text{ nm}$. On the left-hand picture of Fig. 8, the red points present the symmetric efficiencies $(E_{\text{per},\nu'} + E_{\text{per},-\nu'})/2$ depending on the angle $\theta_{\nu'}$ of the propagation direction with $\sin \theta_{\nu'} = \alpha_{\nu'}/k$ (cf. (3.4)). The points of efficiency values are not located, as eventually expected, close to the graph of a smooth function. However, considering smoothed efficiencies (6.13) and simplifying the quasi-interpolation by taking the average

$$E_{\text{per,avg}}(\theta) := \frac{\sum_{\nu': |\theta_{\nu'} - \theta| < \theta_{\text{avg}}} \max\{[\theta_{\text{avg}} - |\theta - \theta_{\nu'}|], 0\} E_{\text{per},\nu'}}{\sum_{\nu': |\theta_{\nu'} - \theta| < \theta_{\text{avg}}} \max\{[\theta_{\text{avg}} - |\theta - \theta_{\nu'}|], 0\}}$$

with average angle $\theta_{\text{avg}} = 10^\circ$, we obtain the smooth curve in green. Note that we multiplied the efficiencies by $\cos \theta$ and a constant. The factor $\cos \theta$ corresponds to the factor p_n in (6.12), and the multiplied efficiency is really a constant multiple of the intensity. The average angle θ_{avg} corresponds

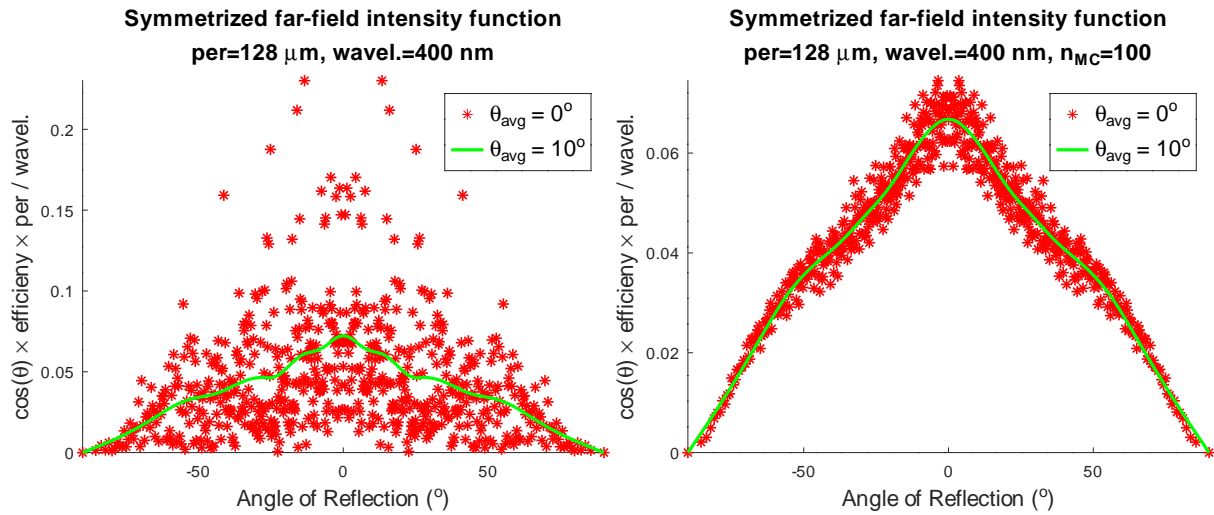


Figure 8: Reflected intensity for a single surface (left) and average of 100 realizations (right).

to the parameter $1/R$ in (6.13). We have tested several values of θ_{avg} starting from 30° going to zero. This results in smooth curves, which do not really change anymore for $\theta_{\text{avg}} \leq 10^\circ$ unless θ_{avg} is so small that the average function follows the jumps of the efficiency points. So $\theta_{\text{avg}} = 10^\circ$ turns out to be a reasonable choice.

In most applications, we are not really interested in a single realization. Think of the roughness of the surface of the ocean or think of the roughness of the planar surface of a workpiece, which ideally should be planar. We are more interested in finding the character of the roughness, i.e., in finding the parameters of the stochastic field modeling the surface. Moreover, it seems natural that our measurement data is not the intensity of the reflection by a single surface but the mean of intensities for many realizations. If we get the measurement data from an air plane flying over the ocean, the sea surface changes with the location or by the time running. If we employ special measurement devices, using beams with “big” cross-section diameter irradiating larger parts of the workpiece and if the aperture of the detector is large, then ergodicity arguments suggest mean values as data. Lastly, if really the reflection of single rough surfaces are measured, then the measurement can be repeated at different places and mean values can be computed. So, following the spirit of the Monte Carlo method, we started to simulate several realizations of the rough surfaces and computed the mean values. Using this, we observe that the average efficiencies on the right-hand picture of Fig. 8 accumulate around the smoothed curve, and the smooth curve looks similar to that on the left-hand side, if the scaling would be harmonized. In our figure, we have used a hundred realizations. Without presenting the pictures here, we mention that the higher the number of realizations, the closer are the red mean values to the points of the smoothed curve (dotted green line).

Now we check the dependence on the period per . There is a rule of thumb to choose the per at least ten times larger than the correlation length \hat{l} (cf. [38, Sect. 2.5]). We generate a big grating with $\text{per} = 128 \mu\text{m}$ or $200 \mu\text{m}$, $\hat{s} = 0.25 \mu\text{m}$, and $\hat{l} = 0.5 \mu\text{m}$ and reduce the period to smaller values by (3.1). Again we fix $\lambda = 400 \text{ nm}$ and $\theta_{\text{inc}} = 0^\circ$. On the left-hand side of Fig. 9, we present the smoothed reflected intensities for various periods and a single representation. On the right we present the intensities for various periods averaged over many representations. The greater the period the closer is the intensity curve to that of the largest period. We remark that an equally good approximation of the intensity can be determined by rough surfaces with huge period and a few number of realizations and by a rough surfaces with period of medium size but with a larger number of realizations (compare Fig. 10 for $\text{per} = 8 \mu\text{m}$ and 10 000 realizations with the left picture of Fig. 8 for $\text{per} = 128 \mu\text{m}$ and 100

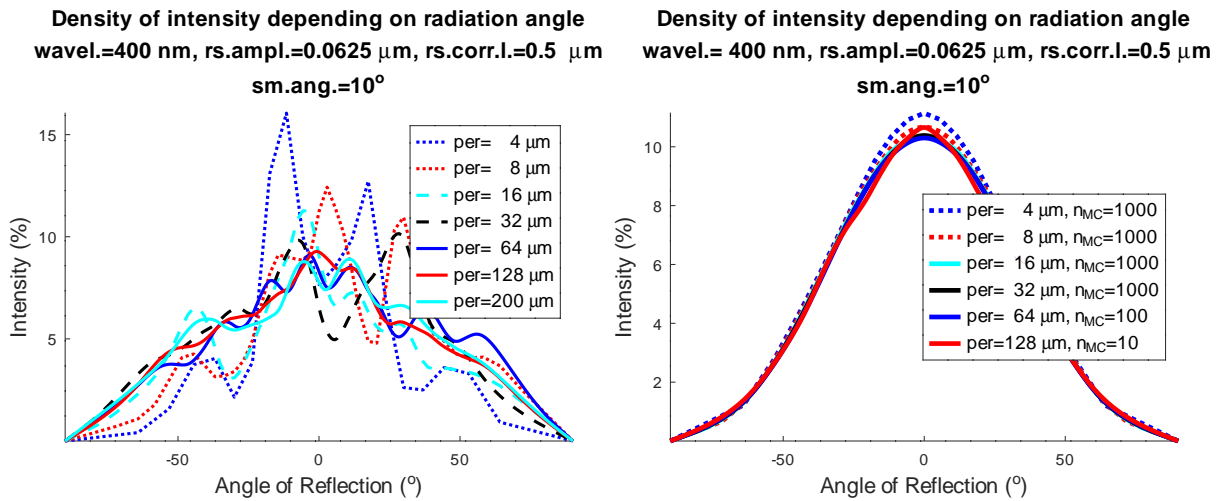


Figure 9: Reflected intensities by periodic approximation of the surface. Single surface (left) and average of many realizations (right)

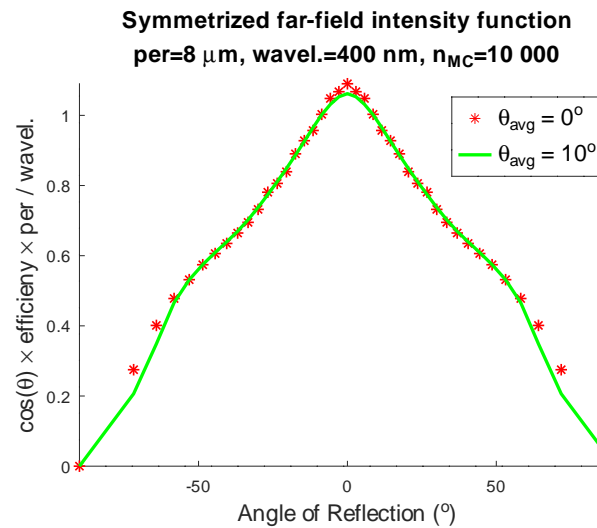


Figure 10: Reflected intensity averaged over 10 000 realizations.

realizations).

Finally, we look at rough surfaces, where an additional plane-wave reflection in accordance to Sect. 6 appears. We generate gratings with per running between 1 μm and 128 μm , fix $\lambda = 400\text{ nm}$, $\theta_{\text{inc}} = 0^\circ$, as well as $\hat{l} = 0.5\ \mu\text{m}$. The additional plane-wave reflection is expected for small corrugations in the roughness, so we choose $\hat{s} = 0.0625\ \mu\text{m}$. For example, in Fig. 11 we choose $\text{per} = 16\ \mu\text{m}$ and see, clearly, the outlier of order zero (propagation angle $\theta_0 = 0^\circ$) for the efficiencies of a single realization on the left and for the average over 1 000 samples at the right. The convergence of the values $E_{\text{per},0}$ and $E_{\text{per,pw}} := E_{\text{per},0} - E_{\text{per},0,\text{sm}}$ (cf. (6.10)) is shown in the plots of Fig. 12 on the left and on the right, respectively.

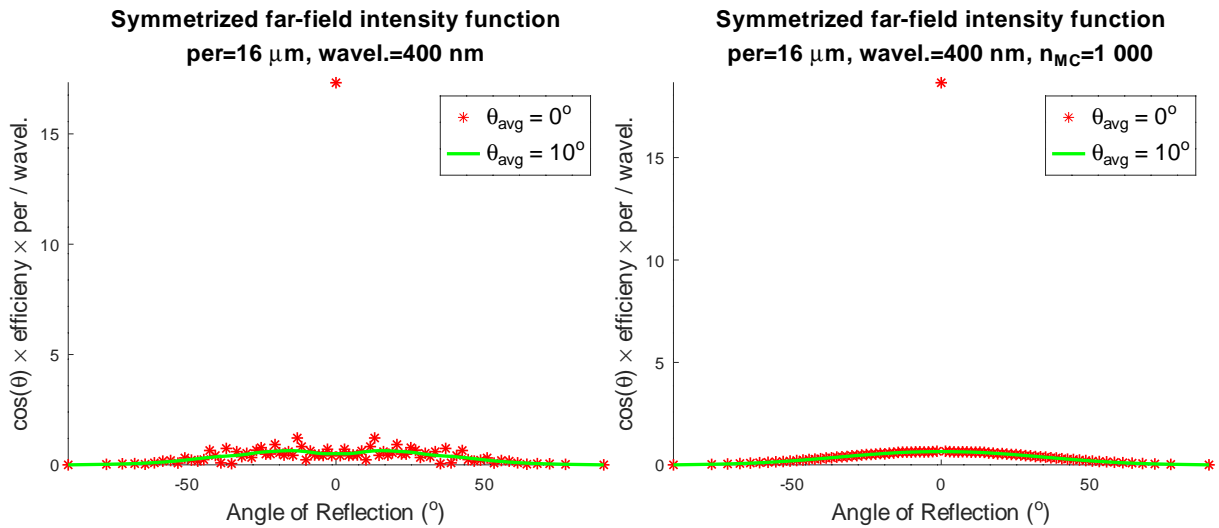


Figure 11: Efficiencies and smoothed efficiencies for rough surface with small amplitudes in the corrugations. For single realization (left) and average over a thousand samples (right).

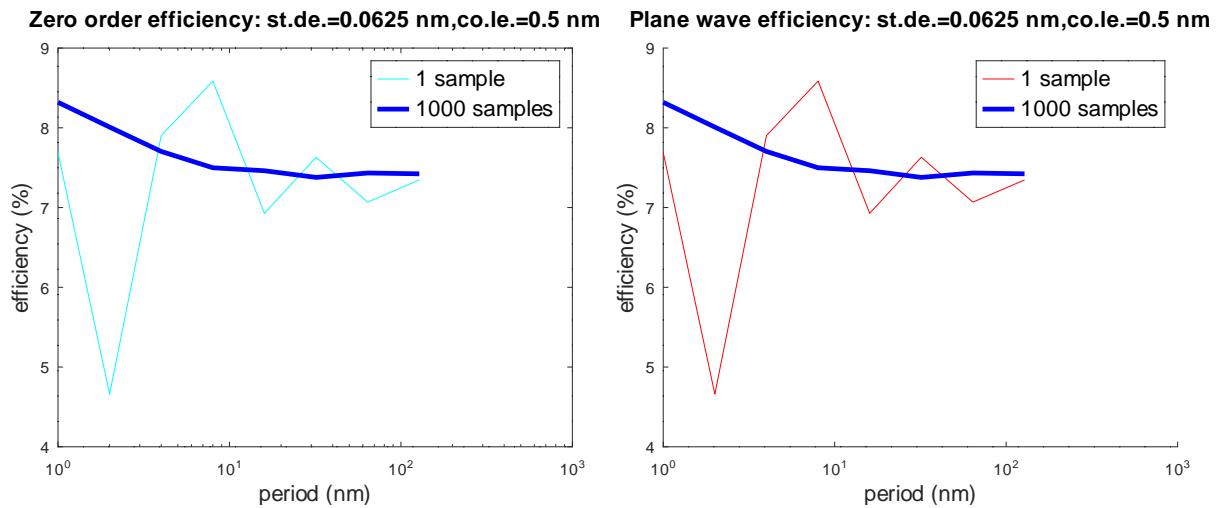


Figure 12: Convergence of the efficiencies for $\text{per} \rightarrow \infty$. Zero order efficiency of periodic surface (left) and efficiency of plane-wave reflection (right).

8 An inverse problem for rough surfaces: Bayesian approach

Now we turn to the inverse problem of reconstructing the random-field parameters of the rough surface from measured scatterometric data, where, as mentioned in Sect. 7, the mean of the usual intensity data is used (cf. [40]). We formulate the problem and report a numerical experiment, where a numerical solution is provided by Bayesian inversion. Note that the measurement setting for the rough surface is just the same as that used for the scatterometric measurement of non-stochastic gratings in [24].

The usual measurement values of the intensity have been introduced in (2.9) and can be simulated by (6.15). Clearly, these values depend on the wavelength λ and on the rough surface, i.e., $I^{\text{meas}} = I^{\text{meas}}(F(\cdot, \omega), \lambda)$ with $F(\cdot, \omega)$ the stochastic realization by the representation (7.1). For an incident wave from above ($\theta_{\text{inc}} = 0^\circ$) with wavelengths $\lambda = \lambda_1, \lambda_2, \dots, \lambda_M$, our measurement data is the vector of the stochastic mean values (expectation, numerically approximated by the mean value

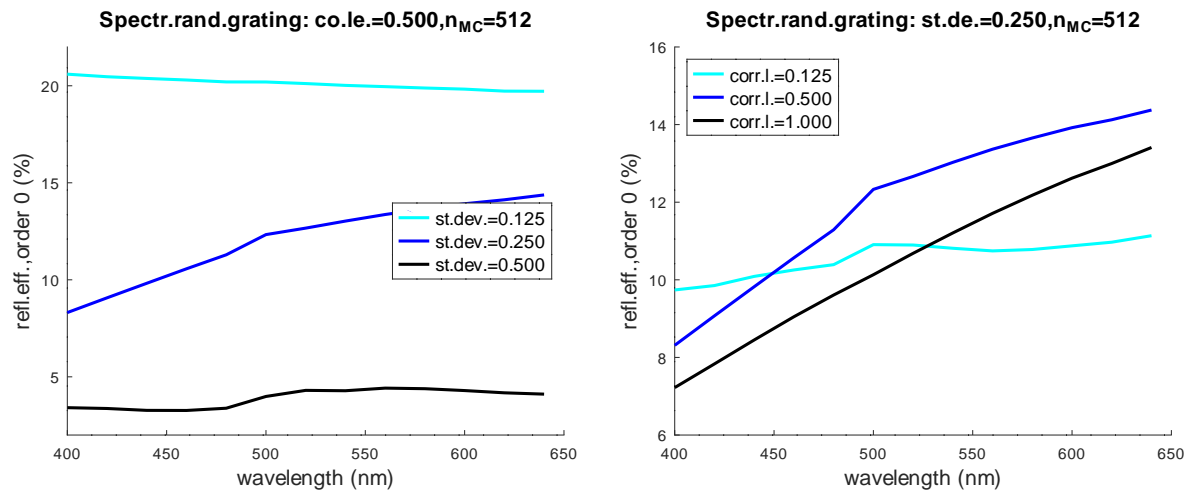


Figure 13: Spectra $\mathbf{E}[E_{\text{per},0'}(\lambda)]$ averaged over $n_{\text{MC}} = 512$ realizations with $\text{per} = 8 \mu\text{m}$ for fixed correlation length $\hat{l} = 0.5 \mu\text{m}$ (left) and for fixed standard deviation $\hat{s} = 0.5 \mu\text{m}$ (right).

over n_{MC} realizations)

$$I_m := \mathbf{E}[I^{\text{meas}}(F(\cdot, \omega), \lambda_m)], \quad m = 1, \dots, M. \quad (8.1)$$

Note that a rough surface can have stochastic corrugations on several “frequency” levels (superposition of random fields with different reciprocal correlation lengths, cf. [38, Sect. 2.2]). The inspecting wave sees only the corrugations, which are close to the wavelength or larger. So it would be natural to adapt the wavelength of the scatterometric measurement to the coarsest corrugations and to reconstruct these first. The unknown data describing the random-field parameters of F , defined by (7.1) or (7.2), is in our simple case the pair (\hat{s}, \hat{l}) of standard height deviation \hat{s} and correlation length \hat{l} .

In more difficult cases the random-field parameters could be a set of parameters describing functions in a class of possible distributions for the i.i.d. random variables $F(x')$ and in a class of possible correlation functions $\mathbb{R}^2 \times \mathbb{R}^2 \ni (x', y') \mapsto \text{corr}(F(x')F(y'))$. Additional unknown parameters could describe the measurement uncertainty, and, in addition to (8.1), one could measure the intensity in several directions or for several directions of incidence. Besides the intensity values, there could be measured phase shifts of the reflected beams or, for electro-magnetic waves, polarization data. However, we restrict our numerical tests to the couple (\hat{s}, \hat{l}) to be recovered from measured data (8.1) with $M = 13$ and $\lambda_m := 400 \mu\text{m} + (m-1)20 \mu\text{m}$. Fig. 13 proves that the spectral data (8.1) is sensitive w.r.t. the stochastic parameters, i.e., to the standard deviation \hat{s} (left) and to the correlation length \hat{l} (right).

To simulate measurement data, we fix the solution $(\hat{s}_{\text{sol}}, \hat{l}_{\text{sol}}) := (0.25, 0.25) \in [0.1, 1] \times [0.1, 1]$ of the inverse problem and compute measurement data for realizations of (7.2) with $\text{per} = 8 \mu\text{m}$ by an FEM method (software package DiPoG, cf. e.g. [14, 20]). In order to avoid unrealistically good reconstruction results, i.e., to avoid the so called inverse crime, we use a very fine FEM grid and a big number of realizations ($n_{\text{MC}} = 4096$) to compute the stochastic mean values. The numerical reconstruction algorithm, which is based on simulations by FEM as well, uses smaller numbers ($n_{\text{MC}} = 128$) for the mean evaluation and coarser FEM grids such that a sufficient accuracy of approximation is reached in an acceptable amount of computing time. In this case the values of \hat{s} are sufficiently large such that the extra plane-wave reflection p_{pw} is zero (cf. Sects. 6 and 7), and the intensity distribution $I_{\text{per},R}^B$ is the smooth $I_{\text{per},R,\text{sm}}^B$ (cf. (6.11)). The latter is the product of a constant times the quasi-interpolant of the efficiency values $E_{\text{per},\nu'}$ (cf. (6.13)). Neglecting the constant, we can assume that the measurement

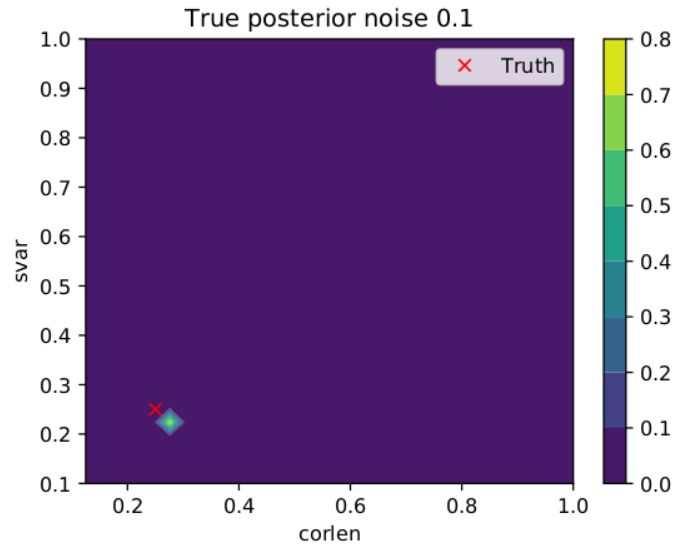


Figure 14: Posterior density $d\pi_\delta$ for noise level $\hat{\eta}=0.1$. Correlation length and standard deviation are given in μm .

values are

$$E_{0'}^{\text{meas}}(\lambda_m) = \mathbf{E}[E_{\text{per},0'}(F(\cdot, \omega), \lambda_m)], \quad m = 1, \dots, M. \quad (8.2)$$

Finally, we replace $E_{\text{per},0'}$ in (8.2) by a noisy $E_{\text{per},0'}^{\text{no}}$, adding a simulated stochastic measurement error to the computed measurement data.

$$E_{\text{per},0'}^{\text{no}}(F(\cdot, \omega), \lambda_m) := E_{\text{per},0'}(F(\cdot, \omega), \lambda_m) + \eta, \quad (8.3)$$

The values of η depend on m and ω . Thus the measurement error η in (8.2)-(8.3) is supposed to be normally distributed without systematic error. The standard deviation $\hat{\eta}$ is the measurement uncertainty, or, in other words, it is the noise level of the measurement.

For the reconstruction of the unknown pair $(\hat{s}_{\text{sol}}, \hat{l}_{\text{sol}})$, i.e., for the solution of the inverse problem, we follow the Bayesian approach (cf. [23]). Choosing the uniformly distributed (non-informative) prior density $d\pi_0(\hat{s}, \hat{l})$ of the values \hat{s} and \hat{l} to be reconstructed from measurement data (8.2), we determine the non-normalized posterior density

$$d\pi_\delta(\hat{s}, \hat{l}) = \exp\left(-\frac{1}{2\hat{\eta}^2} \sum_{m=1}^M \left| E_{0'}^{\text{meas}}(\lambda_m) - \mathbf{E}[E_{\text{per},0'}(\hat{s}, \hat{l}, \lambda_m)] \right|^2\right) d\pi_0(\hat{s}, \hat{l}).$$

Normalizing this to $\frac{1}{2}\pi_\delta([0.1, 1] \times [0.1, 1]) = 1$, for any subset $D \subseteq [0.1, 1] \times [0.1, 1]$ the measure $\frac{1}{2}\pi_\delta(D)$ is the approximate probability that the true solution $(\hat{s}_{\text{sol}}, \hat{l}_{\text{sol}})$ is in D . The plots in the Figs. 14-15 present the scans (30×30 grid points) of the densities of π_δ for the noise levels $\hat{\eta} = 0.1, 1, 10$. The probability measure is concentrated close to the point $(\hat{s}_{\text{sol}}, \hat{l}_{\text{sol}}) = (0.25, 0.25)$. The smaller the noise, the closer are the concentration points to the true solution. Note that even in the best case $\hat{\eta} = 0.1$, there is a deviation from the true solution, which can be attributed to the approximation errors of the FEM and of the mean-value computation.

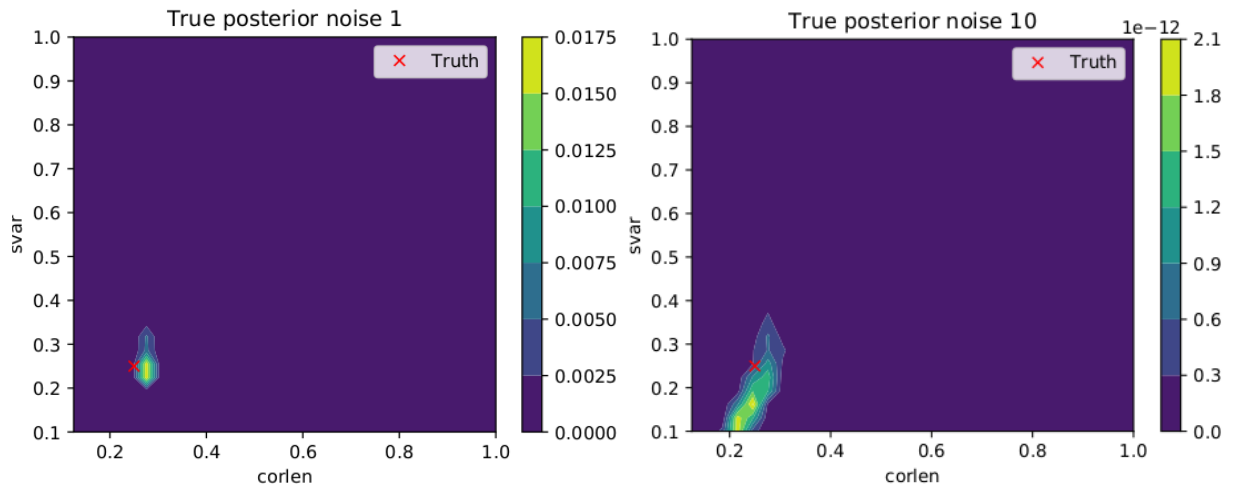


Figure 15: Posterior densities $d\pi_\delta$ for noise level $\hat{\eta} = 1$ (left) and for $\hat{\eta} = 10$ (right). Correlation length and standard deviation are given in μm .

9 Surrogate model by tensor-train representation. MCMC method

Typically, for the solution of the inverse problem, a huge number of FEM simulations is needed. Such a simulation of the observation function, mapping the unknown parameters to the observable measurement values, requires long computation times. This is a problem for our Bayesian inversion and for most of the alternative inverse solvers. It cannot be avoided by using alternative simulation tools like scattering matrix methods (RCWA, FMM) or integral equation methods instead of the FEM. Moreover, if the random-field description is sought for many different surfaces and if the result of the reconstruction is needed in times less than a second (e.g. for in-situ measurements to control a manufacturing process, cf. e.g. [24]), then the simulation should be replaced by a faster surrogate model. The domain of unknown parameters should be scanned, and, for each scanning point a simulation should be performed. Using such a library of simulation values, any further simulation for an arbitrary point in the domain can be replaced by an interpolation of precomputed library values. This is fine for our simple problem with only two unknowns. However, if instead of a single parameter \hat{s} for the normally distributed rough-surface functions F a completely unknown distribution function is sought or if instead of the length \hat{l} of the Gaussian correlation function a generally unknown correlation function is sought, then, after discretization, we end up with many parameters. Due to what is called curse of dimension, a simple computation of a huge library is not possible anymore. A faster algorithm based on adaptive approximation is needed. We suggest a tensor-train approximation (cf. [28]) of the library and show, for our tiny test problem, that such a method works.

The observation is modeled by the mapping $\mathcal{M}: [0.1, 1] \times [0.1, 1] \rightarrow \mathbb{R}^M$, which defines for each (\hat{s}, \hat{l}) the vector of observed (averaged) measurements. To obtain an efficient sampling for the underlying inverse problem, we employ a tensor surrogate $\mathcal{M}_T \approx \mathcal{M}$ (cf. [28] and [15]) which admits a fast evaluation procedure and moderate memory dependency. The approximation \mathcal{M}_T is obtained by an

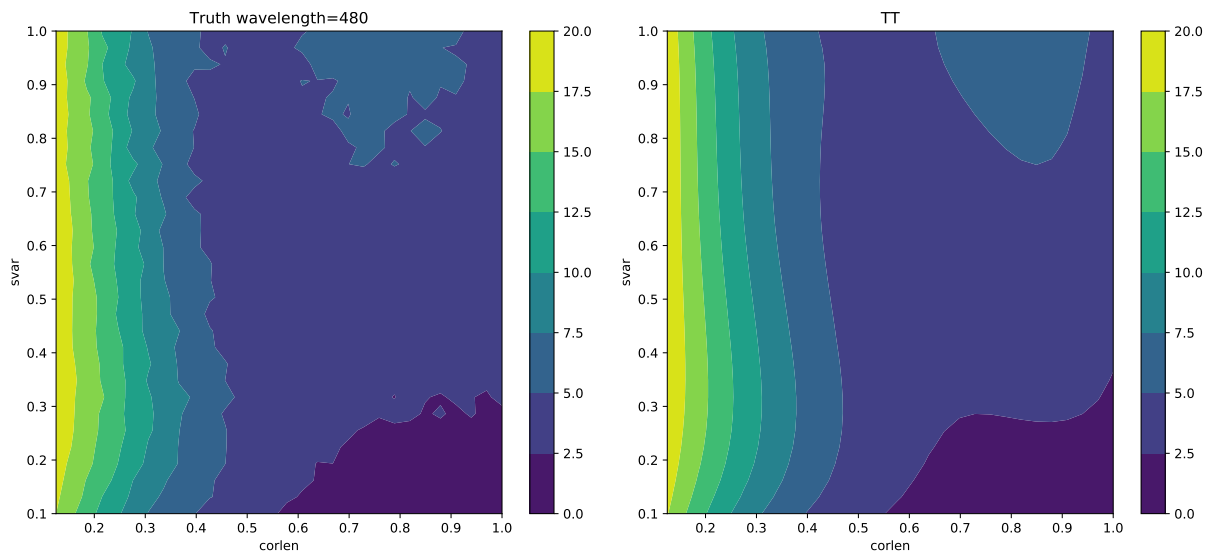


Figure 16: Mapping of observation $\mathcal{M}: (\hat{s}, \hat{l}) \mapsto E_{\text{per},0'}$ for $\lambda_5 = 480$ nm simulated by FEM (left) and surrogate model \mathcal{M}_T of (9.1) (right). Correlation length and standard deviation are given in μm .

optimization approach. For that, the \mathbb{R}^M valued \mathcal{M}_T is modeled as

$$[\mathcal{M}_T(\hat{s}, \hat{l})]_i = \sum_{k_1=1}^{r_1} \sum_{k_2=1}^{r_2} U_0[i, k_1] \left(\sum_{i_1=1}^{n_1} U_1[k_1, i_1, k_2] P_{i_1}^1(\hat{l}) \right) \left(\sum_{i_2=1}^{n_2} U_2[k_2, i_2] P_{i_2}^2(\hat{s}) \right), \quad (9.1)$$

which is a functional extension of the Schmidt or singular value decomposition. In particular, we choose Legendre polynomials for the basis functions P_i^1 and P_i^2 , and fix a low polynomial degree of order $n_1 = n_2 = 5$. Accordingly, the parameter $\mathbf{r} = [r_1, r_2]$ is called rank of the tensor. The component tensors $U_0 \in \mathbb{R}^{M, r_1}$, $U_1 \in \mathbb{R}^{r_1, n_1, r_2}$ and $U_2 \in \mathbb{R}^{r_2, n_2}$ are obtained by minimizing the cost functional

$$\mathcal{J}(U_0, U_1, U_2) = \frac{1}{900} \sum_{i=1}^{900} |\mathcal{M}_T(\hat{s}_i, \hat{l}_i) - \mathcal{M}(\hat{s}_i, \hat{l}_i)|^2,$$

where the (\hat{s}_i, \hat{l}_i) form the points of a uniform grid in $[0.1, 1] \times [0.1, 1]$ (random samples would be suitable as well). The rank parameter \mathbf{r} is chosen adaptively during the optimization procedure.

Even though, the creation of the surrogate model is characterized by an L^2 type minimization, we obtain a favorable convergence in the L^∞ sense due to the regularity of the model \mathcal{M} and due to the compactness of the parameter space $[0.1, 1] \times [0.1, 1]$. The usual choice of Legendre polynomials of order less than five yield a suitable approximation as seen in Figs. 16-17 for $\lambda_5 = 480$ nm. On the left of Figs. 16 the full FEM model is shown. The approximation by the surrogate tensor approximation is on the right and the relative, point-wise approximation error is shown in Fig. 17. The nonsmoothness of the full FEM model does not correspond to a nonsmooth observation function of the true observation function but rather to the nonsmooth approximation by FEM and mean value computation.

The dimension of the tensor representation is given by the amount of degrees of freedom incorporated. Here, for a full tensor representation $Mn_1n_2 = 325$ parameters are needed, whereas in the tensor-train formulation $Mr_1 + r_1n_1r_2 + r_2n_2 = 329$ parameters are used. Actually, this means no model order reduction and is due to the relatively high rank $\mathbf{r} = [8, 5]$. This behaviour can be explained by a high correlation between \hat{s} and \hat{l} w.r.t. the observed quantity. On the other hand, the tensor-train approximation is accurate, and, for higher dimensional versions of the inverse problem, an essential model reduction is to be expected.

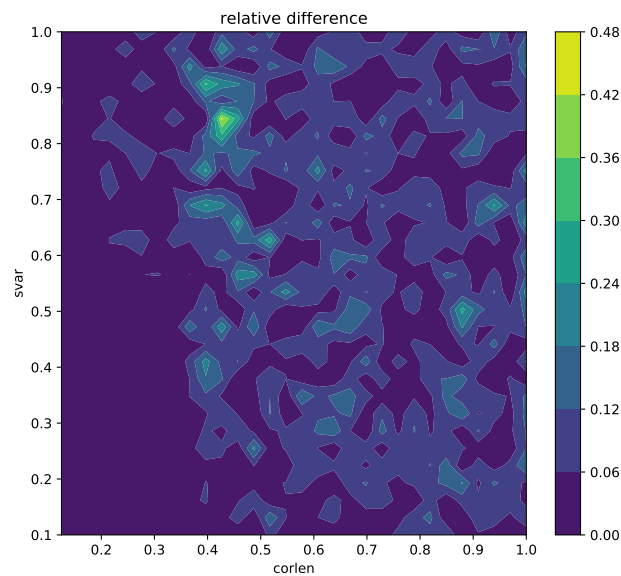


Figure 17: Relative difference of the values in Fig. 16, i.e., of the values simulated by FEM and their approximate values obtained by the surrogate model (9.1). Correlation length and standard deviation are given in μm .

Finally, we consider an alternative way to find the posterior density. Namely, we employ a Markov-Chain Monte-Carlo type algorithm (cf. [5, 16]). For this, the approximate model \mathcal{M}_T is evaluated 8.8×10^5 times (eight chains in parallel over 10^4 samples including a burn in phase of 1 000 samples). This computation was done for the three choices of measurement noise and took about 210 seconds. Note that the computation of the 900 measurements from the true model took about 3 days of computation. The results can be seen in Figs. 18-20. Again, for the low-noise level the true parameter $(0.25, 0.25)$ is correctly recovered with a moderately concentrated posterior density. In the other cases, the estimation is a bit off, but the true parameter lies within the range of a 95% coverage interval.

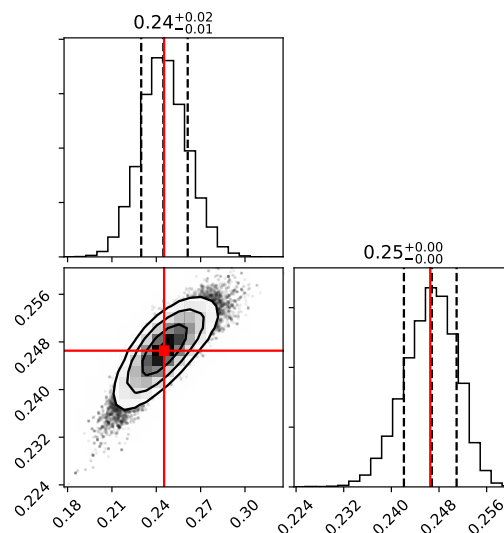


Figure 18: Parameter densities determined by MCMC for noise level $\hat{\eta} = 0.1$. Red lines and marker indicate mean of sample set. Dotted lines correspond to 15% and 85% quantiles. Correlation length and standard deviation are given in μm .

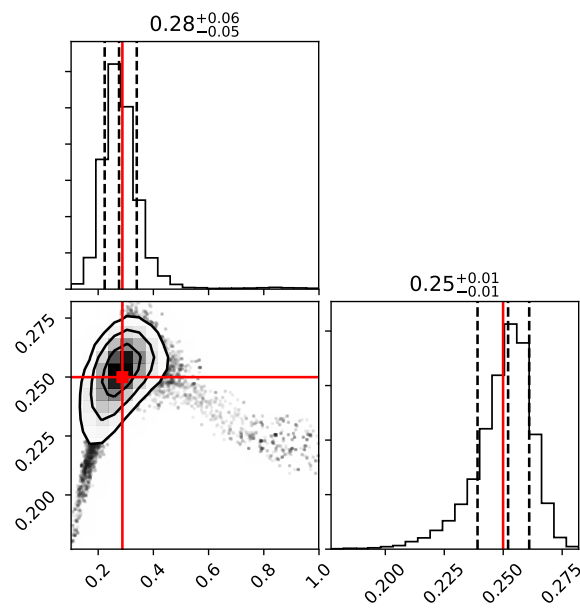


Figure 19: Parameter densities determined by MCMC for noise level $\hat{\eta} = 1$. Red lines and marker indicate mean of sample set. Dotted lines correspond to 15% and 85% quantiles. Correlation length and standard deviation are given in μm .

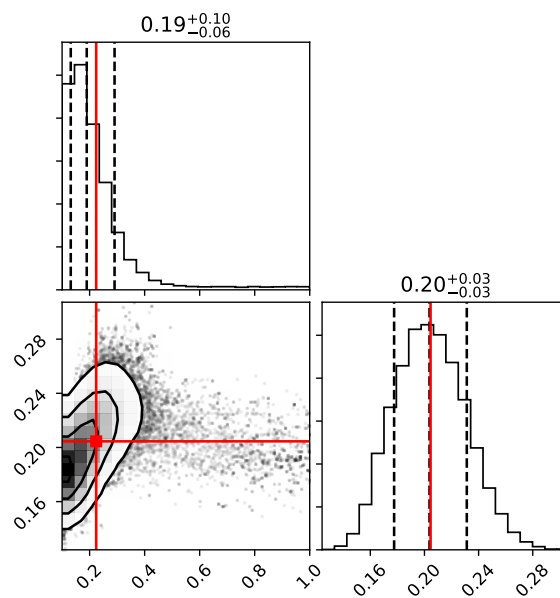


Figure 20: Parameter densities determined by MCMC for noise level $\hat{\eta} = 10$. Red lines and marker indicate mean of sample set. Dotted lines correspond to 15% and 85% quantiles. Correlation length and standard deviation are given in μm .

Acknowledgment

We are grateful to Manuel Marschall for the fruitful discussion and for providing us with the results of the inverse problem, presented in Sects. 8 and 9.

References

- [1] T. Arens and T. Hohage, On radiation conditions for rough surface scattering problems, *IMA J. Appl. Math.* **70** (2005), pp. 839–847.
- [2] T. Arnold and A. Rathsfield, Reflection of plane waves by rough surfaces in the sense of Born approximation, *Mathematical Methods in the Applied Sciences* **37** (14), (2014), pp. 2091–2111.
- [3] P. Beckmann and A. Spizzichino, *The scattering of electromagnetic waves from rough surfaces*, Artech House Inc., Norwood, MA, 1987.
- [4] M. Bieri and Ch. Schwab, Sparse high order FEM for elliptic sPDEs, *Computer Methods in Applied Mechanics and Engineering* **198** (13-14), (2009), pp. 1149–1170.
- [5] S. Brooks, A. Gelman, G. Jones, and X.-L. Meng, *Handbook of Markov chain Monte Carlo*, CRC press, 2011.
- [6] D.H. Chambers (ed.), *Proceedings on the LLNL Workshop on Scattering from Rough Surfaces at Low Grazing Angles (LGA) of Incidence*, Lawrence Livermore National Laboratory: CONF-9405252, 1994.
- [7] S.N. Chandler-Wilde and J. Elschner, Variational approach in weighted Sobolev spaces to scattering by unbounded rough surfaces, *SIAM J. Mathem. Analysis* **42** (2010), pp. 2554–2580.
- [8] S.N. Chandler-Wilde and M. Lindner, Boundary integral equations on unbounded rough surfaces: Fredholmness and the finite section method, *J. Int. Equas. Appl.* **20** (1), (2008), pp. 13–48.
- [9] S.N. Chandler-Wilde and P. Monk, Existence, uniqueness and variational methods for scattering by unbounded rough surfaces, *SIAM J. Mathem. Analysis* **37** (2005), pp. 598–618.
- [10] S.N. Chandler-Wilde, C.R. Ross, and B. Zhang, Scattering by infinite one-dimensional rough surfaces, *Proc. R. Soc. London Ser. A* **455** (1999), pp. 3767–3787.
- [11] S.N. Chandler-Wilde and B. Zhang, A uniqueness result for scattering by infinite rough surfaces, *SIAM J. Appl. Math.* **58** (1998), pp. 1774–1790.
- [12] D. Colton and R. Kress, *Inverse acoustic and electromagnetic Scattering theory*, Appl. Math. Sciences, Vol. **93**, Springer-Verlag, Berlin, Heidelberg, New York, 1998.
- [13] J.A. DeSanto, Scattering by rough surfaces, in *Scattering: Scattering and inverse scattering in pure and applied science*, R. Pike and P. Sabatier, eds., Academic Press, New York, 2002, pp. 15–36.
- [14] J. Elschner, R. Hinder, and G. Schmidt, Finite Element Solution of Conical Diffraction Problems, *Adv. Comput. Math.* **16** (2002), pp. 139–156.

- [15] M. Eigel, R. Schneider, P. Trunschke, and S. Wolf, Variational Monte Carlo - Bridging concepts of machine learning and high dimensional partial differential equations, *Advances in Computational Analysis* **45** (2019), pp. 2503–2532.
- [16] D. Foreman-Mackey, D.W. Hogg, D. Lang, and J. Goodman, The MCMC hammer, *Publications of the Astronomical Society of the Pacific* **125**, (925), IOP Publishing (2013), pp. 306.
- [17] H. Harbrecht, M. Peters, and M. Siebenmorgen, Analysis of the domain mapping method for elliptic diffusion problems on random domains, *Numer. Math.* **134** (4), (2016), pp. 823–856.
- [18] Y. Harness, *Wave scattering by randomly shaped obstacles*, PhD Thesis, Tel Aviv University, Department of Applied Mathematics, 2013.
- [19] R. Hiptmair, L. Scarabosio, C. Schillings, and Ch. Schwab, Large deformation shape uncertainty quantification in acoustic scattering, *Advances in Comput. Maths.* **44** (5), (2018), pp. 1475–1518.
- [20] G. Hu and A. Rathsfeld, Convergence analysis of the FEM coupled with Fourier-mode expansion for the electromagnetic scattering by biperiodic structures, *Electr. Trans. Numer. Anal.* **41** (2014), pp. 350–375.
- [21] G. Hu, W. Lu, and A. Rathsfeld, Time-harmonic acoustic scattering from locally perturbed periodic curves, *SIAM J. Appl. Math.* **81** (2021), pp. 2569–2595.
- [22] L. Li, C.H. Chan, and L. Tsang, Numerical simulation of conical diffraction of tapered electromagnetic waves from random rough surfaces and applications to passive remote sensing, *Radio Sci.* **29** (1994), pp. 587–598.
- [23] J. Kaipio and E. Somersalo, *Statistical and computational inverse problems*, Appl. Math. Sci. **160**, Springer-Verlag, Berlin, Heidelberg, New York, 2005.
- [24] W.M. Klesse, A. Rathsfeld, C. Groß, E. Malguth, O. Skibitzki, L. Zealouk, Fast scatterometric measurement of periodic surface structures in plasma-etching processes, *Measurement* **170** (2021), 108721.
- [25] L. Mandel and E. Wolf, *Optical coherence and quantum optics*, Cambridge University Press, Cambridge, 1995.
- [26] M. Nieto-Vesperinas, *Scattering and diffraction in physical optics*, World Scientific Publishing Co. Pte. Ltd., Singapore, 2006.
- [27] J.A. Ogilvy, *Theory of wave scattering from random rough surfaces*, Adam Hilger, Bristol, 1991.
- [28] I.V. Oseledets, Tensor-train decomposition, *SIAM Journal on Scientific Computing* **33** (5), (2011), pp. 2295–2317.
- [29] H. Ogura and N. Takahashi, Scattering, radiation and propagation over two-dimensional random surfaces, *Progress in Electromagnetics Research* **14**, (1996), pp. 89–190.
- [30] R. Petit (ed.), *Electromagnetic theory of gratings*, Topics in Current Physics 22, Springer-Verlag, Berlin, Heidelberg, New York, 1980.
- [31] A. Rathsfeld, On a half-space radiation condition, *WIAS Preprint* **2669**, Berlin, 2019.

- [32] D.G. Stearns, The scattering of x rays from nonideal multilayer structures, *Journal of Applied Physics* **65** (2), (1989), pp. 491–506.
- [33] D. Sunday, S. List, J. Chawla, and R. Kline, Determining the shape and periodicity of nanostructures using small angle x-ray scattering, *Journal of Applied Crystallography* **48** (5), (2015), pp. 1355–1363.
- [34] L. Tsang, J.A. Kong, and K.-H. Ding, *Scattering of electromagnetic waves: Theory and Applications*, John Wiley & Sons, Inc., New York, 2000.
- [35] L. Tsang, J.A. Kong, K.-H. Ding, and Ch.O. Ao, *Scattering of electromagnetic waves: Numerical Simulations*, John Wiley & Sons, Inc., New York, 2001.
- [36] A. Ulyanekov, Grazing-incidence X-ray diffraction from multilayers, taking into account diffuse scattering from rough interfaces, *Appl. Phys. A* **66**, (1998) pp. 193–199.
- [37] A.G. Voronovich, *Wave Scattering from Rough Surfaces*, Springer, Berlin, 1994.
- [38] K.F. Warnick and W. Cho Chew, Numerical solution methods for rough surfaces, *Waves Random Media* **11**, (2001) pp. R1–R30.
- [39] D.L. Windt, IMD-Software for modelling the optical properties of multilayer films, *Computers in Physics* **12** (4), (1998), pp. 360–370.
- [40] Y.P. Zhao, H.-N. Yang, G.-C. Wang, and T.-M. Lu, Extraction of real-space correlation function of a rough surface by light scattering using diode array detectors, *Appl. Phys. Lett.* **68** (22), (1996), pp. 3063–3065.